INVERSION OF ELECTROMAGNETIC DATA: AN OVERVIEW OF NEW TECHNIQUES

DOUG OLDENBURG

Dept. of Geophysics and Astronomy, U.B.C. Vancouver, Canada, V6T 1W5

Abstract. This paper explores some of the newer techniques for acquiring and inverting electromagnetic data. Attention is confined primarily to the 2d magnetotelluric (MT) problem but the inverse methods are applicable to all areas of EM induction. The basis of the EMAP technique of Bostick is presented along with examples to illustrate the efficacy of that method in structural imaging and in overcoming the deleterious effects of near-surface distortions of the electric field. Reflectivity imaging methods and the application of seismic migration techniques to EM problems are also explored as imaging tools. Two new approaches to the solution of the inverse problem are presented. The AIM (Approximate Inverse Mapping) inversion of Oldenburg and Ellis uses a new way to estimate a perturbation in an iterative solution which does not involve linearization of the equations. The RRI (Rapid Relaxation Inverse) of Smith and Booker shows how approximate Fréchet derivatives and sequences of 1d inversions can be used to develop a practical inversion algorithm. The overview is structured to provide insight about the latest inversion techniques and also to touch upon most areas of the inverse problem that must be considered to carry out a practical inversion. These include model parameterization, methods of calculating first order sensitivities, and methods for setting up a linearized inversion.

Introduction

The development of a computational algorithm which has the ability to easily and robustly extract meaningful information about the conductivity structure of the earth has been a long-time goal of the geophysical community. In the special case when the conductivity structure is a function of depth only, a variety of methods have been proposed and implemented to extract information about $\sigma(z)$ from surface or borehole responses. For those 1d problems however, the number of model parameters and data are generally limited to a hundred or less, and so the matrices involved in linearized approaches are readily manipulated numerically. It seems natural to solve 2d and 3d problems by using the same methods and indeed, much effort has been expended in this regard. Unfortunately, the computational complexity increases dramatically in higher dimensions and this has been a primary reason for slow progress over the last few years. Even in two dimensions, a typical MT survey involving 20 stations produces 10^3 complex responses to be fitted, while the geologic model, when cellularized, may consist of 10^4 or 10^5 parameters. In three dimensions the problem is compounded. Traditional linearized methods therefore require enhanced computing power but the recent availability of super-computers means that substantial progress is being made in this area.

Another technological development available to researchers is the computer workstation with high resolution graphics and considerable computational power. This has opened other avenues for attacking the inverse problem. The data from an electromagnetic experiment constitute a blurred image of the earth structure and consequently the goal of an inversion algorithm can be to generate another image,

Surveys in Geophysics **11**: 231–270, 1990.

not necessarily conductivity as a function of spatial coordinates, which provides information about geologic structure. Image processing, 1d inversions, and accurate 2d forward modelling can be implemented on workstations and such abilities are spawning new approaches in the solution of the inverse problem.

In this paper I will present some of these newer methods and also provide information about more traditional approaches. With respect to traditional approaches to inverting EM data, there already exists a number of excellent reviews. Classic inversion papers by Weidelt (1975) and Jupp and Vozoff (1976) provide a solid foundation for linearized iterative analysis. The review by Varentsov (1983), the comprehensive reference lists given by Hermance (1983) and by Chave and Booker (1987), together with the compendium of papers edited by Vozoff (1986) provide pathways to most literature published up to 1986. A more recent summary of inverse approaches is presented by Hohmann and Raiche (1987). In addition, Whittall and Oldenburg (1900) provide a thorough review for the 1d inverse problem.

I will outline different ways in which surface electromagnetic data can be processed to yield information about electric conductivity and geologic structure. The emphasis will be on the newer techniques. My attention will be focused on the magnetotelluric (MT) problem, and in particular on the 2d problem. Magnetotellurics is an appropriate focus because it includes all of the problems of electromagnetic induction with the exception of spatial variability of the source field (at least in the usual approximation). A thorough understanding of the inversion of 2d MT data will form a solid foundation for solving controlled source problems and the ellusive 3d problem. For the most part, my presentation is ordered according to computational demands of the processing algorithm and, in general, from the least to the most sophisticated algorithms.

A first approach to obtain useful information about the geological structure is to plot the data in various ways. Pseudosection plots can provide immediate insight about the degree of lateral inhomogeneity, and may also provide (to the experienced eye) some indication about the details of the conductivity variation. An image that may provide more direct information about the conductivity structure may be obtained by acquiring electric field data using a contiguous line of dipoles. The resultant data and processing constitute the EMAP technique. This method is new and I will present its basic ideas here. An imaging technique which converts surface-measured impedances into an electromagnetic pseudo-impulse response is presented. Successful imaging provides immediate information about conductivity structure which may be useful in itself, or in a second stage parametric inversion where an acceptable conductivity model is generated. A new iterative inversion method developed by Oldenburg and Ellis (1990) will be presented. Their AIM (Approximate Inverse Mapping) inversion uses accurate forward modelling and an approximate inverse mapping to construct a conductivity model which reproduces the data. The method does not require linearization of the equations or the solution of a large matrix system. Another inversion method which holds great promise is

the Rapid Relaxation Inverse (RRI) of Smith and Booker (1988b). Modified Fréchet derivatives are employed and a 1d inversion is carried out for each station. Both the AIM and RRI methods have a number of impressive computational advantages over generalized linear inverse techniques and are ultimately applicable to the solution of 3d problems. Traditional linearized techniques require the evaluation of 2d Fréchet derivatives or sensitivities. Efficient computation of the sensitivities is necessary to make the approach feasible and I therefore summarize two methods to effect those calculations. Once these first order sensitivities have been developed, standard approaches may be used to iterate toward an acceptable model. Regularization approaches differ and I shall discuss briefly both the statistical formulation of Tarantola (1987) and the construction of models having minimum structure.

Before proceeding, I would like to emphasize that a thorough review of 2d and 3d inversion procedures is too large an undertaking for a single paper (at least for this author), and it is for this reason that I have focused on the 2d magnetotelluric problem. Also, in putting this paper together I have received substantial help from many researchers and my review is correspondingly oriented towards works by those people. Unfortunately, there exist many excellent papers in the literature which are neither reviewed nor referenced in this manuscript. I offer my apologies at the outset to those who have been omitted.

Preamble: Equations and Definitions

The basic equations for EM induction are Maxwell's equations:

$$\nabla \times \mathbf{E} = -\frac{\partial \mathbf{B}}{\partial t} \tag{1a}$$

$$\nabla \times \mathbf{H} = \mathbf{J} + \frac{\partial \mathbf{D}}{\partial t} \tag{1b}$$

$$\nabla \cdot \mathbf{B} = 0 \tag{1c}$$

$$\nabla \cdot \mathbf{D} = \rho_f, \tag{1d}$$

the equation of continuity,

$$\nabla \cdot \mathbf{J} + \frac{\partial \rho_f}{\partial t} = 0, \tag{2}$$

and the constitutive relations:

$$\mathbf{J} = \sigma \mathbf{E}, \quad \mathbf{B} = \mu \mathbf{H}, \quad \text{and} \quad \mathbf{D} = \varepsilon \mathbf{E}, \tag{3}$$

where all quantities are standardly defined (Stratton, 1941: Ward and Hohmann, 1988). At the boundaries between differing conductivities the tangential components of $\mathbf{E}$ and $\mathbf{H}$, and the normal component of $\mathbf{B}$ are continuous; the normal component of $\mathbf{E}$ is discontinuous.

When the conductivity is a function of two coordinates, $\sigma = \sigma(y, z)$, Maxwell's equations decouple if the coordinate axes coincide with directions parallel and perpendicular to strike (the strike direction is chosen to be $\hat{x}$ in this paper). By using Equations (1) and (3), by neglecting the displacement current and assuming harmonic time dependence $e^{i\omega t}$ of the fields, we obtain: the TE (transverse electric) mode equations

$$\begin{aligned} &\frac{\partial^2 E_x}{\partial z^2} + \frac{\partial^2 E_x}{\partial y^2} - i\omega\mu_0\sigma E_x = 0 \\ &H_y = -\frac{1}{i\omega\mu_0}\frac{\partial E_x}{\partial z} \\ &H_z = \frac{1}{i\omega\mu_0}\frac{\partial E_x}{\partial y}, \end{aligned} \tag{4}$$

and the TM (transverse magnetic) mode equations,

$$\begin{aligned} &\frac{\partial}{\partial z}\left(\frac{1}{\sigma}\frac{\partial H_x}{\partial z}\right) + \frac{\partial}{\partial y}\left(\frac{1}{\sigma}\frac{\partial H_x}{\partial y}\right) - i\omega\mu_0 H_x = 0 \\ &E_y = \frac{1}{\sigma}\frac{\partial H_x}{\partial z} \\ &E_z = -\frac{1}{\sigma}\frac{\partial H_x}{\partial y}. \end{aligned} \tag{5}$$

MT data can be characterized in different ways. Two representations of the data will be used here. The TE and TM mode impedances are respectively

$$Z_{xy} = \frac{E_x}{H_y} \quad \text{and} \quad Z_{yx} = \frac{E_y}{H_x}. \tag{6}$$

Apparent resistivities and phase are obtained through the formulae

$$\rho_a = \frac{1}{\mu_0\omega}|Z|^2 \quad \text{and} \quad \phi = \arg(Z), \tag{7}$$

where Z refers to Z_{xy} for TE, and Z_{yx} for TM.

Data acquired at the earth's surface can be thought of as a blurred image of the subsurface geoelectrical structure. A first goal in interpretation is to plot the observations to obtain an image from which geologic structure may be inferred. Plots of apparent resistivities and phases are generally produced. Each of these may provide immediate insight about lateral variability and existence of large scale conductive or resistive structures. In 2d environments Ranganayaki (1984) has shown that apparent resistivity and phase pseudosections derived from the determinant of the impedance tensor may yield semiquantitative information about the conductivity structure.

Unfortunately, the potential insight offered by apparent resistivity pseudosections is often obscured by the 'static' shifts that generally affect field data. Local inhomogeneities near the receiver can cause first-order distortions of the electric field which affect the recovered impedances. At sufficiently long periods, this distortion manifests itself as a multiplication of the apparent resistivity by a constant value. The effects are due to charge buildup and occur only when there is a component of the electric field which is parallel to a conductivity gradient. The impedance phases also provide information about the lateral variability and they have the advantage of not being affected by 'static' shifts. In addition to interpreting phase information directly, it is often advantageous to Hilbert transform the phases to recover apparent resistivity data. In doing this, however, a normalization constant, for example the surface resistivity, is required.

Although information about geologic structure can sometimes be inferred directly from apparent resistivity and phase plots, the extraction of information is hampered for two reasons. The first is due to the near-surface distortions of the electric field referred to above. The second reason is that the conductivity structure is often 3d and complex; data acquired along a single linear array can be difficult to interpret. However, if field data could be acquired and processed to yield directly a simple picture of the conductivity beneath the traverse, then this would be a major step forward. This is the goal of EMAP.

EMAP (ElectroMagnetic Array Profiling)

To overcome the effects of static shifts caused by near surface conductors, F. X. Bostick Jr. (1986) has developed a new approach to acquiring and processing MT data. The modified MT experiment is referred to as EMAP which is an acronym for ElectroMagnetic Array Profiling. The field acquisition involves collecting electric field data using a contiguous set of dipoles along a traverse which can be specified as the $\hat{x}$ direction. The magnetic field is recorded at a single reference site so data are acquired in a Telluric-Magnetotelluric (T-MT) mode. The field observations are reduced via standard methods to compute impedances of the form

$$Z_{xy}(\omega) = \frac{E_x(\omega)}{H_y(\omega)}$$

where H_y denotes the magnetic field in a direction perpendicular to the traverse.

Acquisition of electric field data using contiguous dipoles is fundamental to the technique. For each dipole, an average value of the electric field is obtained by dividing the measured potential difference by the electrode spacing. Since electrode spacing is constant, the observed surface fields are the true electric fields convolved spatially with a box-car averaging function whose width is equal to the electrode spacing. This ensures that electric field data are not spatially aliased.

Further processing is motivated by the following understanding. Consider a near-surface feature of scale length L. An impinging EM field sets up a surface

charge on the body whose magnitude is independent of period if the period is sufficiently long. Electric fields estimated from dipoles with length w where $w \ll L$ will show strong lateral variations when the dipoles are in the vicinity of the charge localization. Conversely, if $w \gg L$ the charges will have minimal effect because the dipole has averaged out the electric field anomaly. It follows that the effect of near-surface conductors is reduced if the effective length of the dipoles is increased. Even though the spacing between field electrodes is small, larger effective spacings are generated by applying a further smoothing to the measured electric fields, or equivalently, to the measured impedances. Bostick advocates the use of a Hanning window whose width is dynamically determined; that is, for each station location and for each frequency, a window is adjusted in accordance with the penetration depth of an EM signal in a medium which has a resistivity equal to the apparent resistivity derived from the smoothed average impedance.

The mathematical justification for the EMAP procedure and further insight into the nature of the required filter is obtained from a linearized analysis of the magnetotelluric problem under the assumption of the Born approximation. This analysis has been outlined in the excellent thesis of Torres-Verdin. A brief summary of highlights from that thesis is provided. The reader is referred to the original thesis, Torres-Verdin (1985), or to papers by Bostick (1986) and Torres-Verdin and Bostick (1988) for more complete details and discussion.

The mathematical development proceeds by first writing the conductivity as $\sigma(x, y, z) = \sigma_0 + \delta\sigma(x, y, z)$ where σ_0 is a constant. The Earth is assumed to be excited by a vertically propagating plane wave with time dependence $e^{i\omega t}$. By breaking the field into primary and secondary components as

$$\mathbf{E}(\mathbf{r}) = \mathbf{E}_p(\mathbf{r}) + \mathbf{e}(\mathbf{r}), \tag{8}$$

one can write the differential equation for the secondary electric field as the inhomogeneous Helmholtz equation

$$\nabla^2\mathbf{e} - i\omega\mu_0\mathbf{e} = i\omega\mu_0\delta\sigma\mathbf{E} \tag{9}$$

for which a solution may be written in terms of a dyadic Green's function as

$$\mathbf{e}(\mathbf{r}) = \int_V G(\mathbf{r} \mid \mathbf{r}_0) \cdot \mathbf{E}(\mathbf{r}_0)\delta\sigma(\mathbf{r}_0)\, \mathrm{d}v. \tag{10}$$

To linearize the equations, it is first assumed that the conductivity perturbation is small; that is, $|\delta\sigma| \ll \sigma_0$. With this assumption, the scattered fields are small and the total electric field in (10) may be replaced by the primary inducing field. Let the inducing field be

$$\mathbf{E}_p(\mathbf{r}_0) = \hat{x}E_{x_0}\, e^{-ikz_0}. \tag{11}$$

Then only the first column of the dyadic Green's function becomes important and (10) reduces to

$$e_j(\mathbf{r}) = \int_{\tau_0} G_{j1}(\mathbf{r} \mid \mathbf{r}_0)E_{x_0}\, e^{-ikz_0}\delta\sigma(\mathbf{r}_0)\, \mathrm{d}\tau_0 \tag{12}$$

where $j = 1, 2, 3$ delineates $\hat{x}, \hat{y}, \hat{z}$ components. Define the spatial Fourier transform with respect to x and y to be

$$e_j(\xi, \eta, z) = \int_x \int_y e_j(x, y, z)\, e^{-i(\xi x + \eta y)}\, dx\, dy.$$

Taking the 2d transform of (12) and making use of the fact that $G_{j1}(\mathbf{r} \mid \mathbf{r}_0)$ depends upon $(\mathbf{r} - \mathbf{r}_0)$ yields

$$e_j(\xi, \eta, z) = \int_{z_0} E_{x_0}\, e^{-ikz_0} G_{j1}(\xi, \eta, z \mid 0, 0, z_0) \delta\sigma(\xi, \eta, z_0)\, dz_0. \tag{13}$$

The spatially Fourier transformed secondary fields at the surface $z = 0$ can therefore be written as

$$e_j(\xi, \eta, 0) = \int_{z_0} K_j(\xi, \eta, z_0) \delta\sigma(\xi, \eta, z_0)\, dz_0. \tag{14}$$

The characteristics of the kernel function K_j for $j = 1$ (that is, for evaluating the electric field in the direction of the inducing field) are given below for the cases of 1, 2, and 3 dimensional structures.

1d:

$$K_1(0, 0, z_0) = \frac{\omega\mu_0\sigma_0}{k}\, e^{-i(k+k)z_0} \tag{15a}$$

2d (E parallel to strike):

$$K_1(0, \eta, z_0) = \frac{\omega\mu_0\sigma_0}{\zeta}\, (r_1)\, e^{-i(\zeta+k)z_0} \tag{15b}$$

2d (E perpendicular to strike):

$$K_1(\xi, 0, z_0) = \frac{\omega\mu_0\sigma_0}{\zeta}\, (1)\, e^{-(\zeta+k)z_0} + \frac{\xi^2}{i\zeta}\, e^{-(\zeta+k)z_0} \tag{15c}$$

3d:

$$K_1(\xi, \eta, z_0) = \frac{\omega\mu_0\sigma_0}{\zeta}\, (r_2)\, e^{-(\zeta+k)z_0} + \frac{\xi^2}{i\zeta}\, e^{-(\zeta+k)z_0}. \tag{15d}$$

In the above

$$\zeta = (k^2 - \xi^2 - \eta^2)^{1/2} \tag{16}$$

is the vertical wavenumber and

$$k^2 = -i\omega\mu_0\sigma_0. \tag{17}$$

The absolute value of the complex reflection coefficients r_1 and r_2 is bounded according to

$$\tfrac{1}{2} \leqslant |r_1| \leqslant 1 \quad \text{and} \quad \tfrac{1}{2} \leqslant |r_2| \leqslant 1. \tag{18}$$

It is seen that all kernels in Equation (15) have a first term which behaves as

$$\frac{\omega\mu_0\sigma_0}{\zeta} \operatorname{Re}^{-i(\zeta+k)z}. \tag{19}$$

Variability in the amplitude and the phase of this term for the four kernels arises from differences in the vertical wavenumber of the scattered field and in the value of a (complex) reflection coefficient R. Note that the premultiplying amplitude coefficient depends upon ω/ζ and thus Equation (19) goes to zero as frequency goes to zero.

The 2d TM and 3d kernels however, have an additional term whose amplitude is proportional to ξ^2/ζ. For specified horizontal wavenumbers and for sufficiently small frequencies, this quantity approaches a constant. If the decay term in the exponent is small, i.e. the depth z_0 under consideration is small compared to the skin depth of the incident wave, then the exponential term will be of appreciable size. Under these conditions, the second term in Equations (15c–d) will be appreciable and will accordingly amplify any wavenumber component of the conductivity perturbation at that depth. It is this effect which gives rise to the static shift observed in MT data.

Realizing that this second term is a source of difficulty, it follows that more interpretable MT data may be obtained if its effect could be removed. Ratioing the two terms in Equation (15c) shows that the second term is smaller than the first if

$$\xi^2 \ll \omega\mu_0\sigma_0. \tag{20}$$

It follows that the 'static' component, which predominates at high horizontal wavenumbers, can be attenuated by applying a spatial digital filter in the $\hat{x}$ direction.

The main difficulty in applying this filter is to ensure that the data to be filtered have been initially sampled in accordance with the sampling theorem, i.e. the data were not aliased upon acquisition. This can be assured if the electric fields are acquired from a contiguous line of dipoles. In such a scheme, each voltage represents an average value of the electric field over the distance between the electrode positions. If data are recorded in this manner, further filtering is easily effected. Bostick chooses to use a Hanning window for low passing. The window is

$$w(x) = \begin{cases} \dfrac{1}{L}\left(1 + \cos\left(\dfrac{2\pi x}{L}\right)\right), & |x| \leqslant L/2 \\ 0, & |x| > L/2 \end{cases} \tag{21}$$

where L specifies the length of the window and is to be determined. If the Earth were a halfspace, then Equation (20) suggests that

$$L \gg \frac{1}{\sqrt{\omega\mu_0\sigma_0}}$$

or

$$L = \beta\sqrt{\frac{\rho_0}{\omega\mu_0}} \tag{22}$$

where β is a constant to be specified by the interpreter. Values in the order of one to three are reasonable. With the choice of L given in Equation (22), the electric field at the surface will be smoothed over a spatial length that is related to the skin depth of the wave in the medium. In practice, the appropriate value of the halfspace conductivity is not available (there is no halfspace) and L is selected to be proportional to the apparent skin depth for the frequency in question. Let $w_i(L)$ denote the weights for the Hanning window of length L. The smoothed impedance at location x_j and frequency ω_k is

$$\bar{Z}_{jk} = \bar{Z}(x_j, \omega_k) = \sum_{i=-l}^{l} w_i Z(x_{j-i}, \omega_k). \tag{23}$$

The EMAP apparent resistivity is

$$\bar{\rho}_{ajk} = \frac{1}{\mu_0 \omega_k} |\bar{Z}_{jk}|^2 \tag{24}$$

and the desired length is

$$L_{jk} = \beta \sqrt{\frac{\bar{\rho}_{ajk}}{\mu_0 \omega_k}} = \frac{\beta}{\mu_0 \omega_k} |\bar{Z}_{jk}(L)| . \tag{25}$$

If L_{jk} is not equal to the value of L used to generate the Hanning weights, then the weights are recalculated using L_{jk} and the procedure is iterated until a consistent smoothing length is achieved.

There is no doubt that the application of this technique to 2d structures (and probably to 3d structures) produces significant attenuation of near-surface static distortions. An example is presented in Figure 1. Numerous other examples by Bostick show similar improvements. Moreover, the EMAP image is often indicative of the geologic structure. This is especially true when the geology consists of a few (perhaps dipping) layers with simple buried bodies or thrust zones. It seems therefore that the images observed in EMAP processed data may well provide significant information about geologic structure.

Having established the importance of EMAP in attenuating near-surface effects and in structural imaging, the next question that arises is concerned with how to get further quantitative information from EMAP data. Looking again at the kernels in Equation (15) we see that if the static terms are attenuated then only the first, frequency-dependent term remains. Although the terms for all kernels are similar in form, there are significant quantitative differences caused by variability in the vertical wavenumbers and in the reflection coefficients; these can produce substantial quantitative differences between the kernel values. There are further complications. EMAP data are acquired only by measuring the electric field in a direction parallel to the traverse direction. Within the Born approximation, the electric fields perpendicular to this direction should not produce significant fields in the direction parallel to the traverse. In practice, however, conductivity contrasts can be large, and the Born approximation will not be valid. All statements made in conjunction

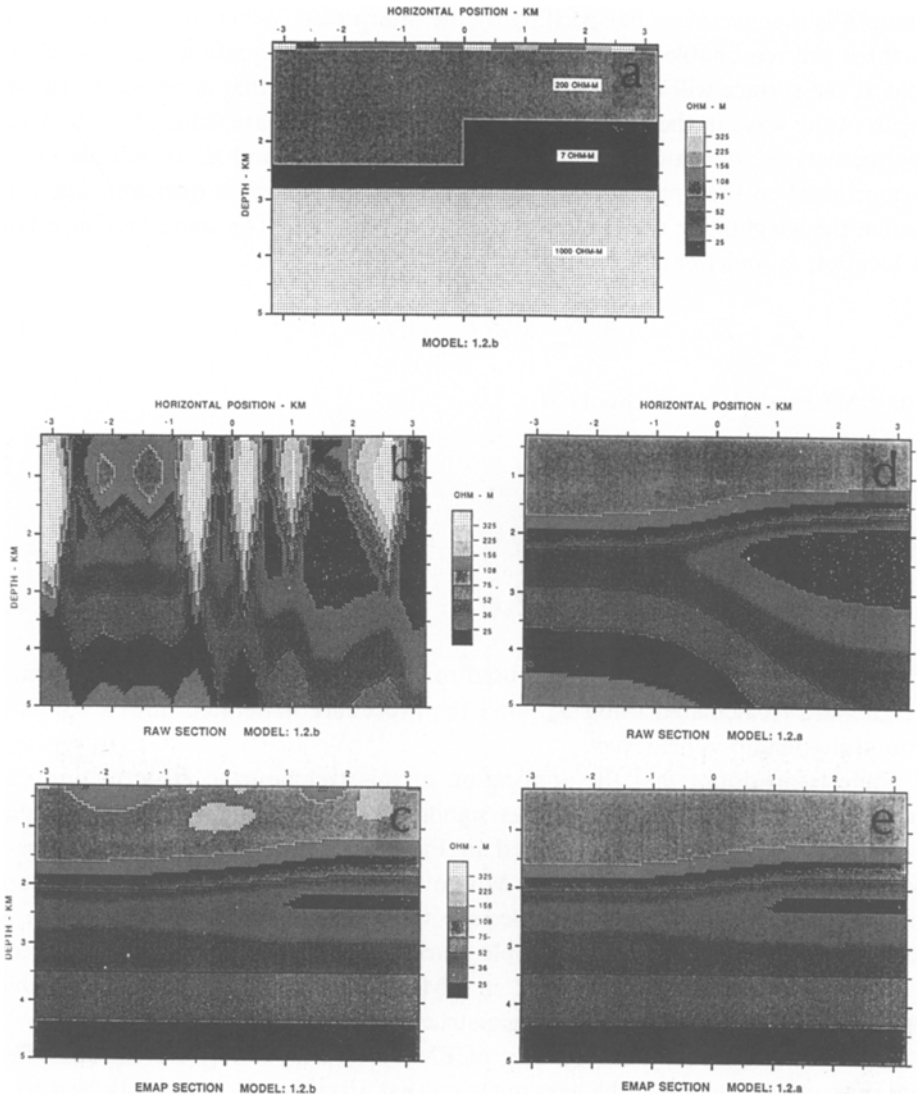

Fig. 1. The conductivity model with a near surface chaotic zone is shown in (a). The apparent resistivities obtained from forward modelling are shown in (b) and the EMAP processed data are shown in (c). Panels (d) and (e) are the forward modelled apparent resistivities and the EMAP data when the variable surface layer in (a) is replaced by a layer with resistivity 200 $\Omega \cdot$ m. The panels are taken from advertisements supplied by Advanced Energy Technology Inc.

with the Born approximation will fail to some extent and the magnitude of the consequences will be unknown.

To obtain some insight about quantitative aspects of EMAP data, the EMAP processing is applied to 2d MT data generated from a conductive prism buried in a halfspace. This idealistic model is shown in Figure 2a. The original and processed data are displayed as gray scale panels in Figure 2b–e. The apparent resistivities in

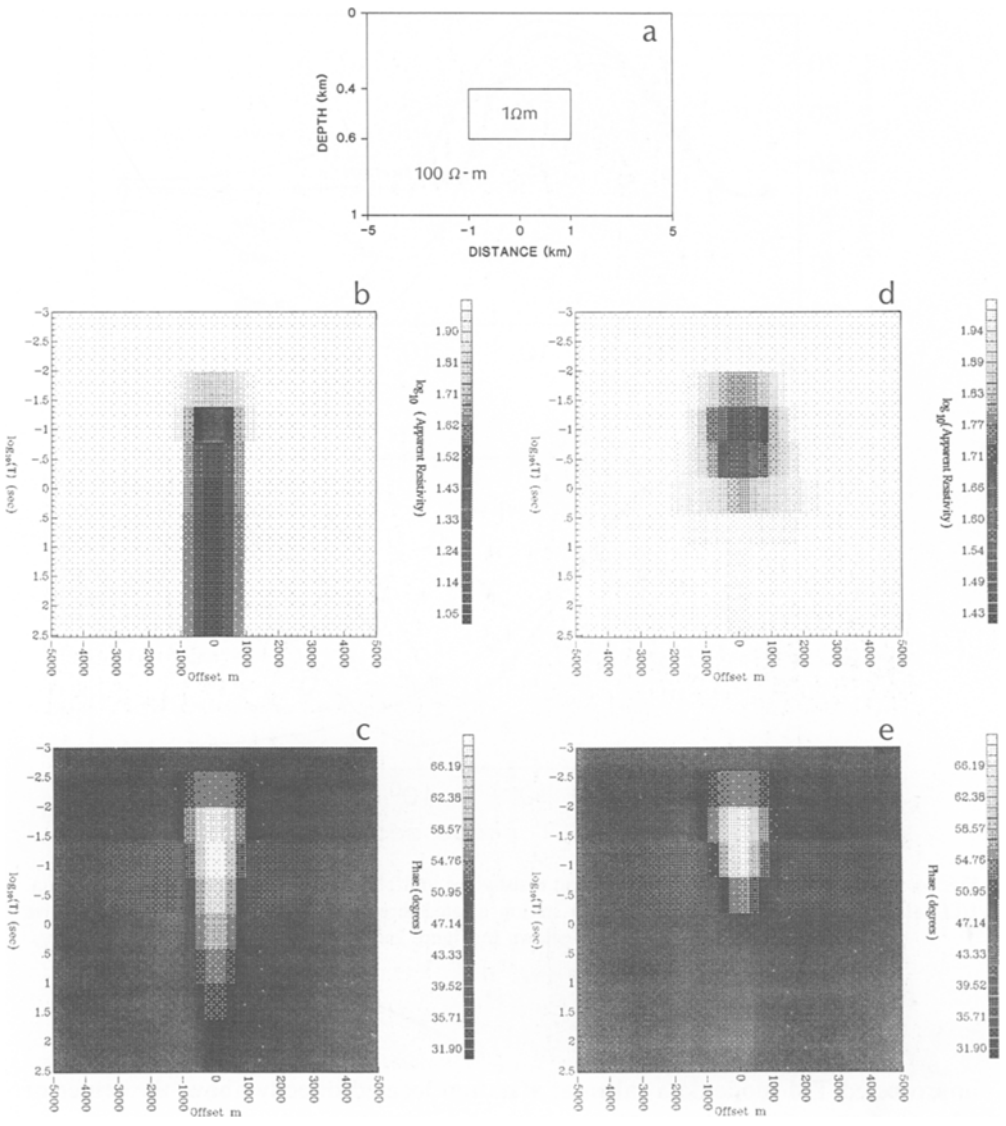

Fig. 2. The conductivity model is shown in panel (a). The TM mode apparent resistivity and phase are shown in panels (b) and (c). The finite element modelling code of Wannamaker *et al.* was used to generate the forward responses. EMAP processing applied to those data yields the images in (d) and (e).

Figure 2b show the drop out caused by charge density buildup along the boundaries of the block. As shown in Figure 2d, this undesirable feature is eliminated by EMAP processing and thus, from a geologic imaging perspective, EMAP is successful. Figure 2e shows that the general character of the phase pseudosection is not greatly altered by the processing. These are positive aspects of EMAP processing. More quantitatively however, Figure 3 shows profiles of the processed and

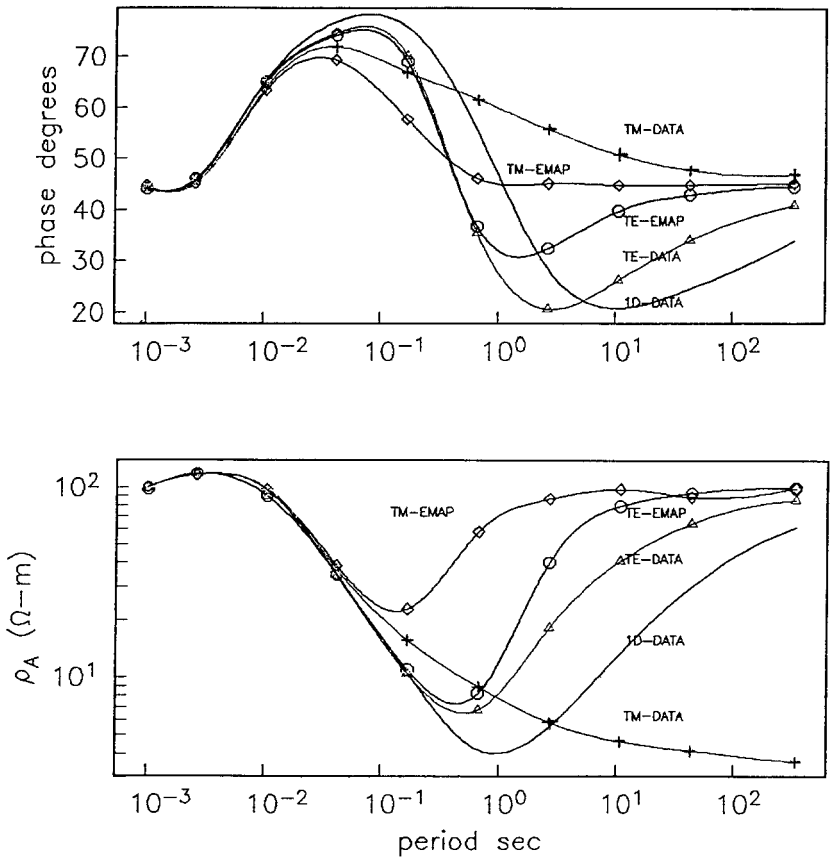

Fig. 3. Quantitative comparison of apparent resistivities and phases for 2-D TE and TM mode data, 1-D data, and EMAP processed data for a station located directly over the centre of the conductive prism shown in Figure 2a.

unprocessed TM mode data taken at a station located directly above the center of the prism. Also plotted are the responses from a 1d model corresponding to the conductivity beneath the station, the 2d TE responses, and the output of applying the EMAP processing to the TE mode data. The latter was done because within the context of the Born approximation, EMAP processing should not significantly alter TE mode data. It is conceded that the processing carried out here may not be optimum; a value of $\beta = \sqrt{2.0}$ was chosen for all stations and for all frequencies. Nevertheless, it appears that the EMAP data cannot be interpreted as either the 1d or 2d TE mode data as might have been envisaged originally. It follows that further inversion of the processed data must proceed by incorporating directly the fact that each EMAP datum is a smoothed impedance. This appears to be an area of fruitful research.

Reflectivity Formulation to Recover Structure

A number of inversion techniques proposed over the years regularize the problem by introducing a simple geologic parameterization for the earth model. Conductivities, and perhaps layer or block boundaries, are adjusted so that predicted data and observations agree. The success of such algorithms depends upon the initial parameterization.

To pursue this approach it would be helpful if the structural geometry could be determined directly from the field data. The full inversion could proceed in two phases; the first would generate the parameterization, the second would create a valid conductivity model. Essentially, this philosophy follows that used in reflection seismology where reflection seismograms are processed to produce a stacked section on which correlatable events are interpreted as reflections from an interface. Inversion follows as a subsequent processing step. Kunetz (1972), Loewenthal (1975), Szaraniec (1976) and others have expounded upon the mathematical similarity of the 1d EM induction equation and the wave equation. To exploit this relationship, Levy et al. (1988) used a linear programming approach to construct a pseudo-impulse response for MT data. In their method, apparent resistivities and phases are used as input to a linear inverse problem and the constructed time function is made up of discrete pulses whose amplitudes depend upon the electromagnetic reflection and transmission coefficients at various layer interfaces. The arrival time of an individual pulse corresponds to the time for a reference signal to travel a particular raypath from the surface to the reflector and back. The display of the impulse responses recovered from many stations produces an MT reflectivity section from which geologic structure may be inferred.

To summarize the essential steps, consider a 1d layered earth and a vertically propagating plane wave source with a time dependence $e^{i\omega t}$. Displacement currents, as usual, are neglected. The earth is parameterized so that $\sqrt{\sigma}h$, (root conductivity and the layer thickness) is a constant for each layer. This Goupillaud parameterization (Goupillaud, 1961), requires that for a given frequency ω, the amplitude attenuation of the wave and the time required for the wave to travel through the layer, will be the same for each layer. The discretization for the problem is therefore specified by choosing the physical parameters σ_1 and h_1 for the first layer.

Let $t_0 = \sqrt{\mu_0 \sigma_1} h_1$. Physically t_0 has the dimensions of $\sqrt{sec}$, but numerically its value corresponds to the two-way traveltime (in seconds) of an EM wave with angular frequency $\omega = 2$ propagating through a medium of thickness h_1 and conductivity σ_1. Introducing

$$u = e^{-2\sqrt{i\omega}t_0} \tag{26}$$

and following standard procedures (Loewenthal, 1975, Claerbout, 1976) it is straightforward to show

$$R(\omega) = \sum_{m=1}^{\infty} q_m u^m = \sum_{m=1}^{\infty} q_m e^{-2\sqrt{i\omega m}t_0}. \tag{27}$$

The series of coefficients $\{q_m\}$ in (27) represents the 'time-domain' impulse response for the EM plane wave. The $\{q_m\}$ series is not directly analogous to the observed surface EM fields that would arise from an impulsive plane-wave source. Rather, it is the response obtained when all aspects of wave attenuation and dispersion have been removed. The series is therefore called a 'pseudo-impulse' response. This response depends upon the reflection and transmission coefficients for a layered earth.

The relationship between the mathematical form of the response in (27) and the measured impedances is given by

$$R(\omega) = \frac{1}{2}\left(\sqrt{\frac{\sigma_1}{i\omega\mu_0}}\, Z(\omega) - 1\right). \tag{28}$$

Equations (27) and (28) form the basic relationship between the measured data and the pseudo-impulse response. If $R_j \equiv R(\omega_j)$ is known at N different frequencies, then $2N$ real constraints exist on the infinite sequence $\{q_m\}$. A particular solution corresponding to a minimum structure conductivity model is obtained by minimizing

$$\Phi = \sum_{m=1}^{\infty} |q_m|$$

subject to fitting the data constraints.

A simple numerical example corresponding to 2 layers over a halfspace is shown in Figure 4. Thirteen data in the frequency range 0.1 to 1000 Hz were used to recover the pseudo-impulse response shown in trace 3 of Figure 4d. The times of the impulse events are consistent with waves traversing the raypaths shown in panel (e).

Although the mathematics is developed for a 1d earth, the technique can be applied to recover information about 2d conductivity structure. In areas where the earth is composed of dipping layers or smoothly varying lateral boundaries, it is expected that the impulse response section will yield direct information about 2d structure. In cases where lateral variation is extreme and 2d effects are manifest, then the recovered $\{q_m\}$ series will contain these effects and further processing will have to be done before the true geologic structure is revealed.

An application of the method to a 2d structure simulating a salt dome is shown in Figure 5. TE mode responses were generated using a finite element program provided by Wannamaker *et al.* (1985) and the inversion was carried out by allowing a 10% relative error misfit on each observation. The recovered reflectivity image features three reflection events on the left-hand side of the dome corresponding to three conductivity discontinuities there. Only two reflections are observed on the right; this is in accordance with the conductivity model. The high amplitude negative reflection (event 5) is the primary event from the top of halfspace. The large travel time pullup of event 5 for traces in the center of the image is caused by the high velocity of EM waves as they travel through the resistive salt.

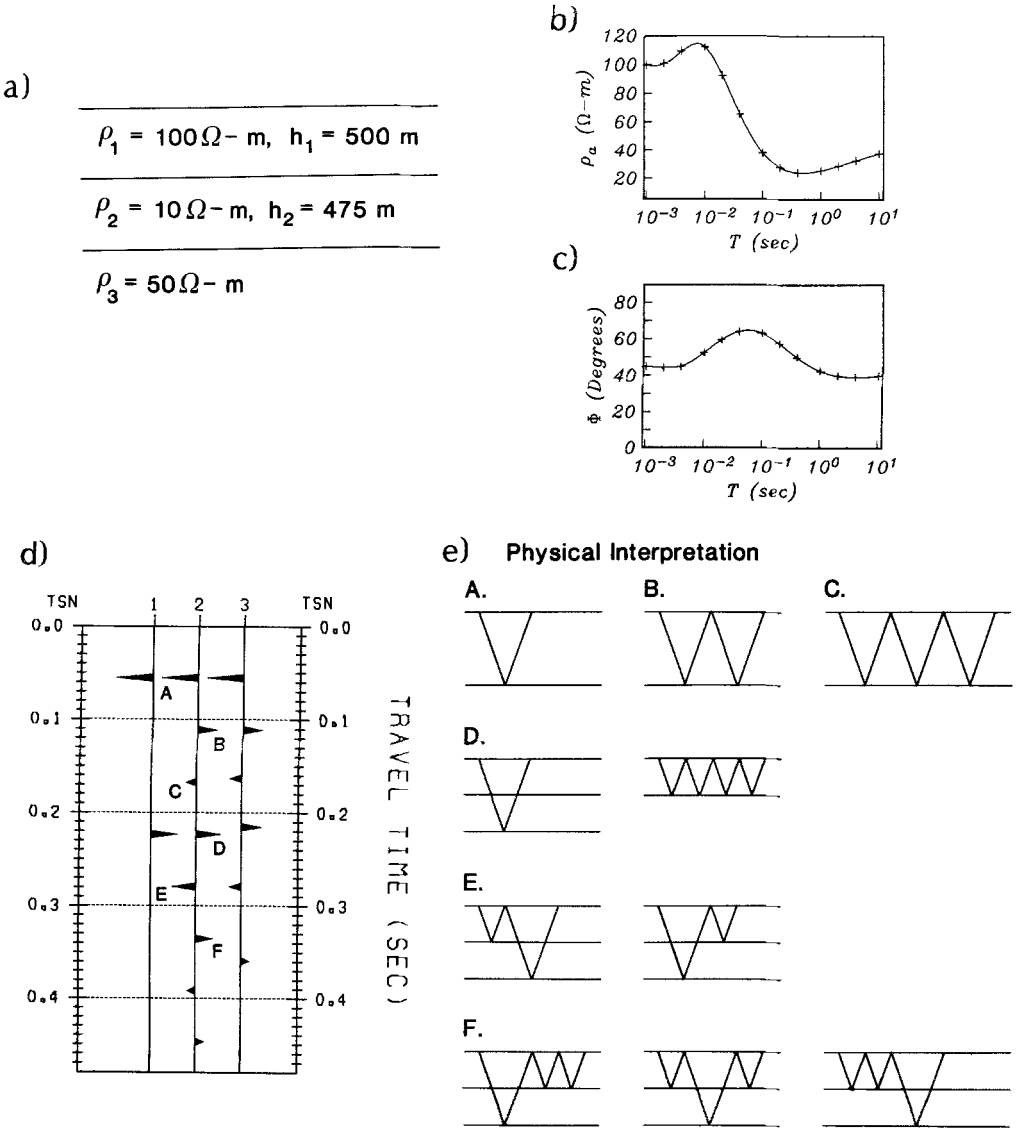

Fig. 4. A layered model is shown in (a). Apparent resistivities and phases are given in (b) and (c). The traces in (d): (1) the primary reflectivity series; (2) the theoretical pseudo-impulse response series; and (3) the recovered impulse response series obtained by inverting the apparent resistivities and phases in (b) and (c). The physical interpretation of the events observed on the pseudo-impulse response series is shown in (e). Events (D), (E) and (F) are composite events made up of arrivals of energy following different paths.

Although this imaging approach has great intuitive appeal, it is not without difficulties in practical application. Successful recovery of an interpretable impulse response depends both upon choice of norm to be minimized (that given in equation (29) may not suffice for some geologic structures) and the degree of accuracy to which the data equations are fit. The non-uniqueness, inherent in

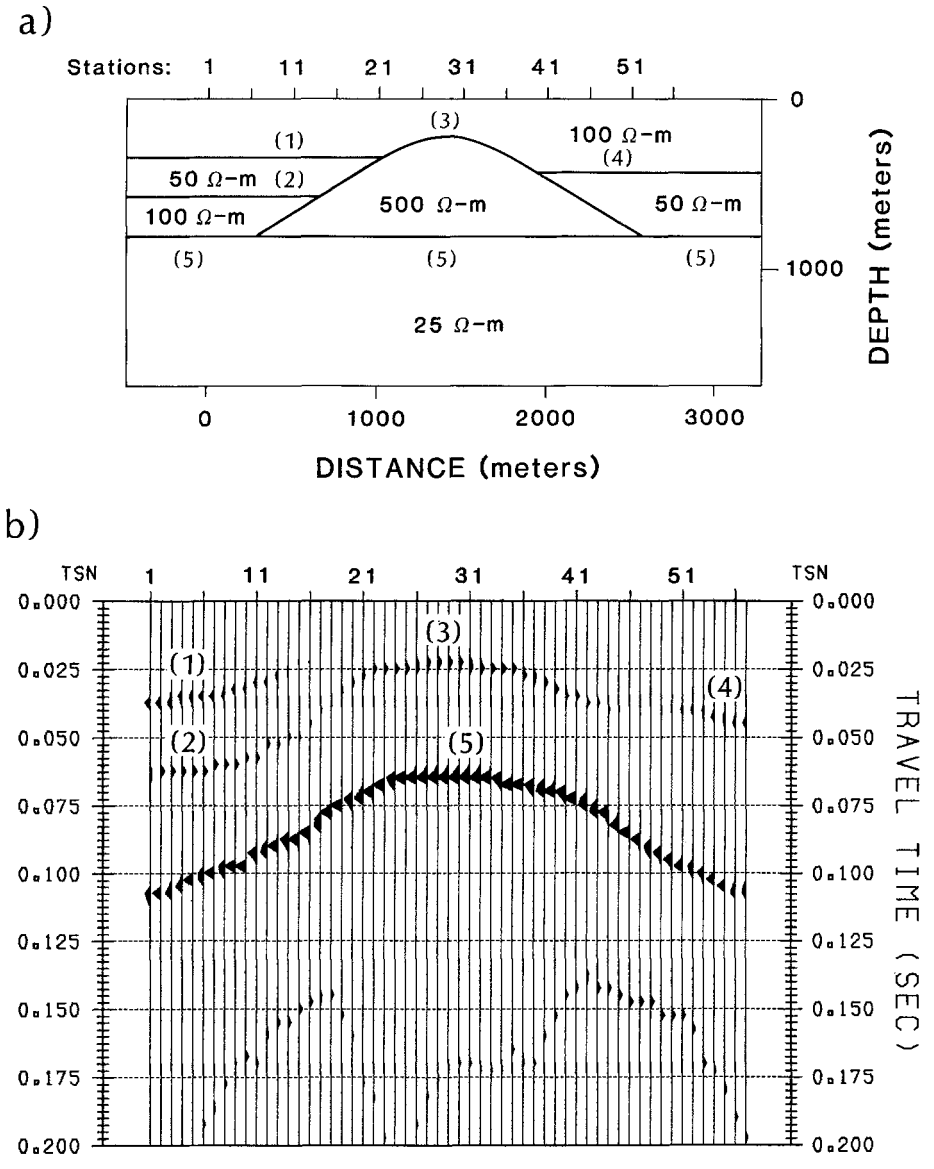

Fig. 5. A 2-D conductivity structure simulating a resistive salt dome buried in a layered medium is shown in (a). The EM reflectivity time section obtained by inverting the TE mode data is shown in (b). Events (1)–(5) are reflections from corresponding interfaces in (a). The only event requiring additional explanation is (5), a primary reflection from the top of the halfspace. The large traveltime decrease arises because of the high resistivity (and therefore large velocity) of the salt formation.

estimating a function whose moments with exponentially decaying kernel functions constitute the observed data constraints, is ever present.

There have been other approaches which make use of the similarity between seismic and EM waves. In all cases the goal has been to process the EM data to recover information about structure or relative conductivity. The most thorough

and sophisticated studies in this regard have been pioneered by Zhdanov and his coworkers. In this first method Zhdanov and Frenkel (1982, 1983) developed an electromagnetic migration technique that is applicable for transient electromagnetic data. The Stratton-Chu integrals are used to back-propagate the observed surface fields through a medium of specified conductivity. These fields are imaged at any value of reversed time and these images delineate the locations of anomalous currents or charges. The method has been successfully applied to interpreting MHD sounding date from the Kola Peninsula (Velikhov *et al.*, 1987).

The second method offered by Zhdanov (1987) is really a recipe for solving the inverse problem; the imaging portion is but an intermediate step. Observed frequency domain data are first separated into normal and anomalous fields and these latter fields are further disected into near surface and deep parts. The techniques outlined in Berdichevsky and Zhdanov (1984) are used to downward continue the deep anomalous fields. The shapes of the downward continued fields localize the anomalous conductivity structure and therefore guide the parameterization for a subsequent inversion. Application of the technique to data from the Carpathian region appears to have been successful.

In an approach which is intimately related to Zhdanov and Frenkel's electromagnetic migration, Lee *et al.* (1987) downward continue surface observed **E** and **H** fields to recover a 2d resistivity image of the substructure. Their work is a direct parallel to seismic migration and they use the one-way wave equation and an assumed background conductivity to back-propagate the waves. The algorithm is implemented in the frequency domain and independent images of relative conductivity are obtained by processing **E** and **H** pseudosections separately. In order for their algorithm to work, it is required that the background conductivity be known and that the conductivity contrasts are small so that multiple reflections can be ignored. They also require data from a large number of closely spaced stations and at many frequencies. Nevertheless, the results of synthetic examples presented in their paper were quite successful and the method deserves further research.

Specification of the Model and the Data

Plotting the data, applying reflectivity or electromagnetic migration imaging, or carrying out EMAP processing may produce significant insight about geologic structure. Generally however, more quantitative information is desired from a formal inversion method to determine a conductivity model which adequately reproduces the observed data. The fundamental questions to be asked are 'what is the model', and, 'what are the data?' These need to be explicitly defined because it is the compatibility between the (possibly processed) data and the assumed mathematical model that permits quantitative inversion to be effected. If the geology is modelled as a 2d structure, then either it must be 2d, or the data should be processed so that 3d effects are minimized. Accomplishing the latter task is not easy.

In defining the mathematical model, one needs to specify the parameterization. Many options are possible. The model may be parameterized so that a few major features are sought. For example, the model might consist of a number of buried bodies embedded in a halfspace or in a 1d background conductivity structure. Justification for this may come from geologic knowledge, from EMAP results or from reflectivity imaging. The earth model may also be descretized into many individual cells and the inverse problem formulated so as to find a minimum structure conductivity model which reproduces the data.

As in 1d inversions, there is never a best method of parameterization which is applicable to all problems. Parameterizations which yield underdetermined systems of equations offer the greatest flexibility in model construction but the characteristics of the computed model are dictated by the model norm to be minimized. While a particular choice (for instance minimizing the curvature of the conductivity) may produce a good description of the true conductivity structure for a particular data set, it may be totally incorrect for another data set. The electromagnetic inverse problem is nonunique. Geologically meaningful answers can be obtained only when all available information and intuition are incorporated into the inversion. This is where insight from plotting the data, EMAP results, reflectivity imaging, geologic information, and well control can aid significantly.

In certain investigations, it makes geologic sense to model the earth as a set of major discrete units. The inverse problem is solved for parameters which specify the conductivity interior to each unit (cellular values or parameters of a specified function). The location of block boundaries may also be included as formal parameters. This hybrid model has been adopted by numerous authors including Zhdanov and Golubev (1983), Park (1987), Mackie *et al.* (1988) and Wannamaker (personal communication).

As a guiding philosophy one should always attempt to reduce the mathematical model to as few parameters as are required to yield a reasonable geologic description of the earth. All information available should be used to guide the parameterization, but it must be remembered that incorrect parameterization means that the earth model can never be recovered. When in doubt about the parameterization, it is generally better to discretize the earth structure as finely as computing practicalities dictate, incorporate geologic/geophysical constraints directly in the inversion, and regularize by finding a minimum norm solution.

I now turn to the question of 'what are the data?' At the time of writing this review, most quantitative inverse attacks are directed towards the 2d inverse problem. If a 2d model is adopted, then the effects of 3d earth conductivity variations will cause difficulties in the inversion. The problem is compounded by the short spatial wavelength of some variations. This is made apparent by comparing the responses from nearby stations. In Figure 6 I have plotted the responses for two pairs of MT stations located near Nelson, B.C. in the southern Cordillera. The station locations are shown in Figure 6e. The data were acquired by Jones *et al.* (1988). The maximum distance between adjacent stations is 500 m, yet the

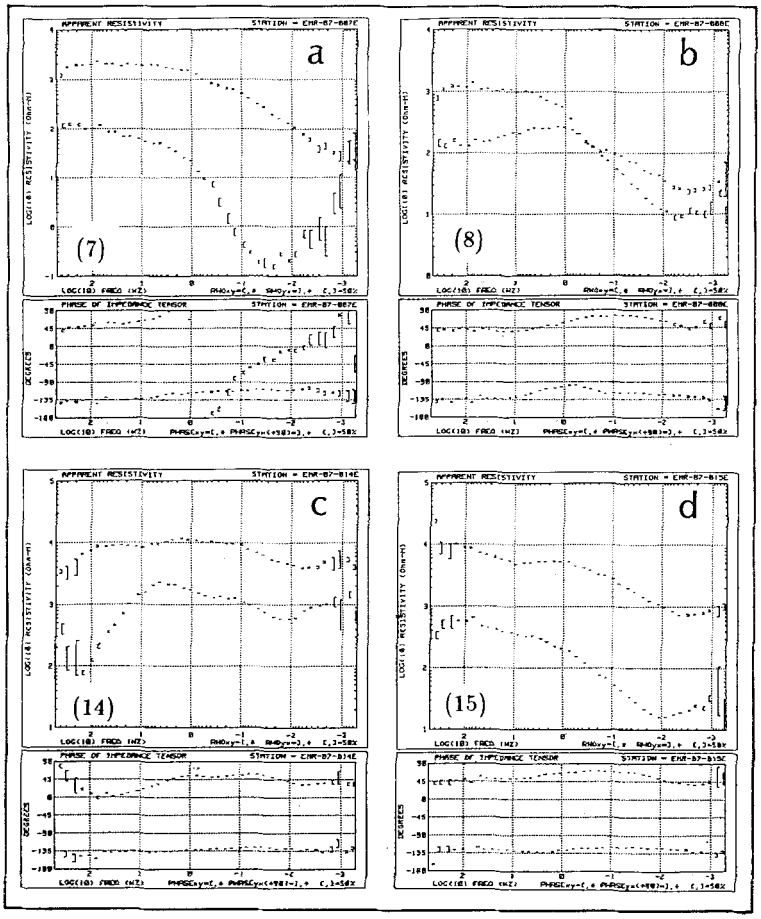

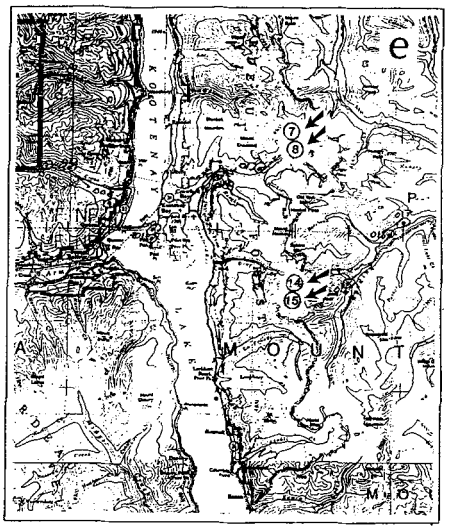

Fig. 6. Panels (a)–(b) and (c)–(d) display MT data taken near Neslon, British Columbia, Canada. Each pair of stations is separated by about 500 m. Locations of the stations are shown in panel (e).

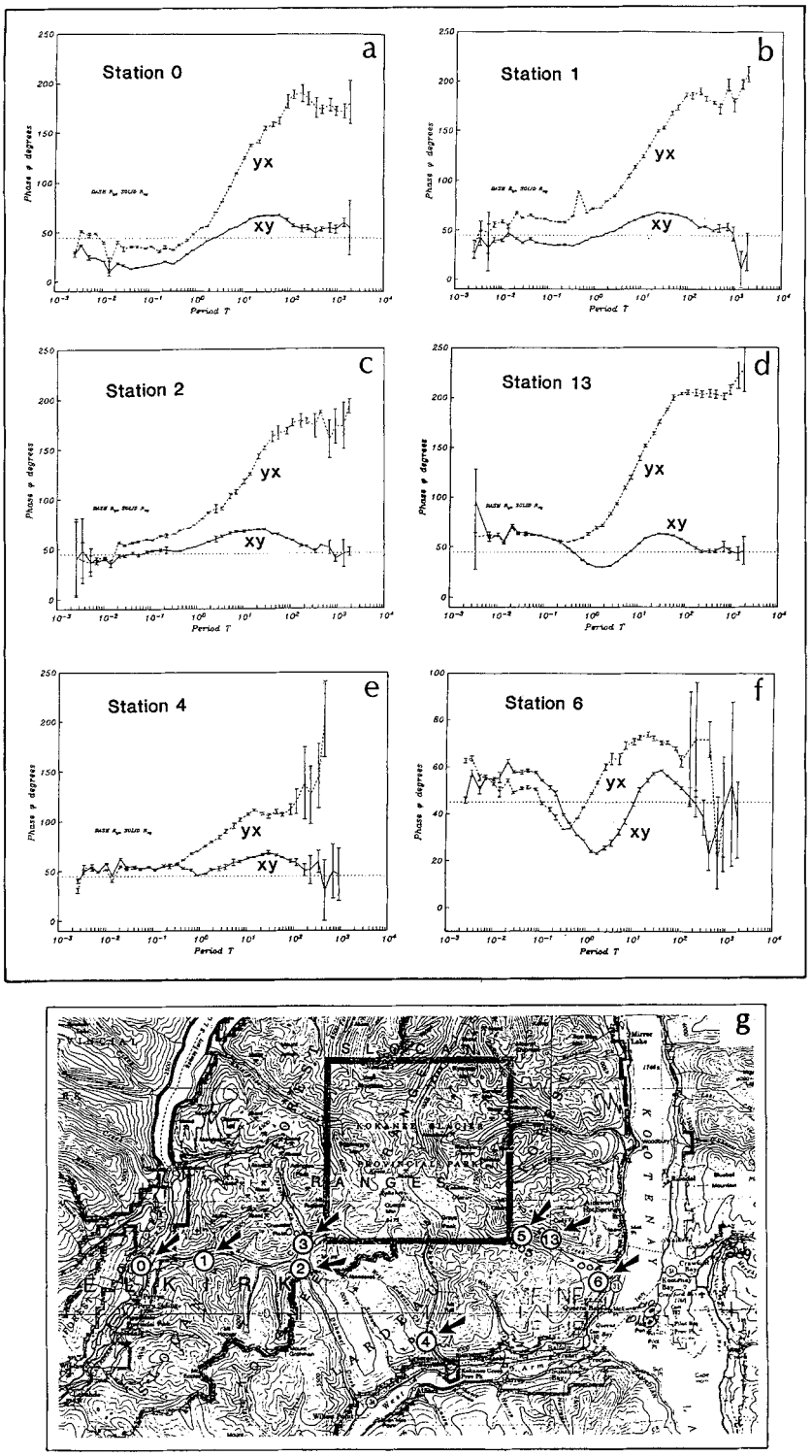

Fig. 7. MT data having anomalous phases in the *yx* component are shown in panels (a)–(e). Phase excursions of 135° are consistent across the array. The data were acquired by Jones *et al.* (1988) on the Nelson Batholith in British Columbia, Canada. Locations of the stations are shown in panel (g).

responses are highly dissimilar. Presumably the variability is caused by large distortions of the surface electric field and of course, it is this variation that EMAP attempts to suppress. From the point of view of inverse modelling however, these results are disconcerting and the question, 'which features of the data at adjacent stations should be reproduced?', is left unanswered.

In less extreme cases there may be a geological reason for assuming that a 2d inversion will be approximately valid. Regarding the question of 'what are the data?', Wannamaker *et al.* (1984), based upon results of forward modelling, have argured that it it best to use a 2d TM modelling algorithm if the profiles of apparent resistivity and phase are centrally located across elongate, geometrically regular 3d bodies. The vertical magnetic field can also supply essential information about the conductivity and it should be included if possible (eg Kurtz *et al.* (1986)). An alternative approach however, is to attempt to fit simultaneously both modes of data and tipper information (if possible). Because of the inconsistency between the earth model and its mathematical representation, only the major characteristics, and not individual small scale features of the data, should be fit. The validity of this latter approach depends upon the magnitude of the 3d effects and upon how closely a 2d structure can be expected to emulate 3d responses. If the discrepancies are extreme, then the suggestion by Wannamaker *et al.* (1984) may be better.

Before leaving the subject of data specification, I offer another example of difficult data. Data taken by Jones *et al.* (1988) on the Nelson Batholith show anomalous phases in one of the components. Phase variations extend over 135 degrees and yet are extremely consistent across the array (see Figure 7). These phase excursions are not unique to the Nelson Batholith. Similar phases were encounted by Flores *et al.* (1985) in a survey at Meagre mountain. To my knowledge such phase variation is not a predictable response from 3d structures. This suggests that it may be the result of processing or that our exploration in forward modelling 3d data has been too limited. Whichever, the hope of inverting these data cannot be entertained until explanation of the anomalous phases is at hand.

Approximate Inverse Mapping

I now turn attention to the problem of generating a 2d conductivity structure which fits the observed data. Many approaches can be applied; a usual approach linearizes the equations and uses the 2d Fréchet derivatives to compute a perturbation step in an iterative solution. Although this approach may ultimately have an advantage in being able to fit precise details of the data, it is computationally demanding. Moreover, in any linearized scheme, the Fréchet derivatives are evaluated at the current model and hence accurate computation of 2d sensitivities is not warranted in the early stages of model construction; other simpler approaches may yield equally good or better perturbation steps.

One possible approach is the Approximate Inverse Mapping (AIM) technique proposed by Oldenburg and Ellis (1990). They use an approximate inverse mapping in conjunction with accurate 2d forward modelling to construct a conductivity perturbation. They present two basic ways to do this. In one of their methods, and the one I will illustrate here, the approximate inverse mapping is applied both to the observations and to the predicted responses; the model perturbation is obtained by subtracting the two results.

The approximate inverse mapping is ideally chosen to incorporate the major physics of the problem. For a 1d inversion, the approximate inverse mapping can be derived from asymptotic equations which show that vertical conductance is the controlling factor in the attenuation of EM data. In 2d problems the approximate inverse mapping may be selected as a composite of 1d inversions carried out at each station. There is no need to linearize the equations in the AIM inversion and hence the computation of the sensitivity matrix and the need to solve a large matrix system of equations are obviated. As a consequence, the inversions are easily carried out on a computing workstation.

The AIM approach is iterative. Let $m^{(0)}$ denote the starting model and let $m^{(n)}$ be the model constructed at the n'th iteration. Let $\mathcal{F}$ denote the forward mapping (a precise 2d forward modelling algorithm in this case) and let $\tilde{\mathcal{F}}^{-1}$ denote the approximate inverse mapping.

Application of the forward mapping produces the predicted responses

$$\mathcal{F}[m^{(n)}] = e^{(n)}. \tag{30}$$

Application of an approximate inverse mapping $\tilde{\mathcal{F}}^{-1}$ yields a model which is denoted by a tilde:

$$\tilde{\mathcal{F}}^{-1}[e^{(n)}] = \tilde{m}^{(n)}. \tag{31}$$

At the nth iteration we desire to find a perturbation $\delta m^{(n)}$ which, when added to $m^{(n)}$, reproduces the data. That is

$$m^{(n+1)} = m^{(n)} + \delta m^{(n)}, \tag{32}$$

and

$$\mathcal{F}[m^{(n+1)}] = e^{\text{obs}}. \tag{33}$$

Since the inverse mapping is approximate, it is not expected that its application to $e^{(n)}$ would reproduce $m^{(n)}$. Denote this mapping error by

$$\begin{aligned} \Delta m^{(n)} &= m^{(n)} - \tilde{\mathcal{F}}^{-1}[\mathcal{F}[m^{(n)}]] \\ &= m^{(n)} - \tilde{m}^{(n)}. \end{aligned} \tag{34}$$

If the updated model $m^{(n+1)}$ is expected to reproduce the observations, then the mapping error $\Delta m^{(n+1)}$, obtained by combining Equations (33) and (34), can be written as

$$\Delta m^{(n+1)} = m^{(n+1)} - \tilde{m}^{\text{obs}}. \tag{35}$$

Applying (32) yields

$$\delta m^{(n)} = \tilde{m}^{\text{obs}} - m^{(n)} + \Delta m^{(n+1)}.$$

An assumption is required in order to proceed. $\Delta m^{(n+1)}$, the 'error' in the inverse mapping for the updated model, is not known, but if we assume the mapping errors at the n'th and $(n+1)$'th models are approximately the same, then

$$\Delta m^{(n+1)} \simeq \Delta m^{(n)} = m^{(n)} - \tilde{m}^{(n)}$$

and the final perturbation is

$$\delta m^{(n)} \simeq \tilde{m}^{\text{obs}} - \tilde{m}^{(n)}.$$

Oldenburg and Ellis (1990) explore a number of possible inverse mappings. The basic criterion is that the approximate inverse mapping incorporates the major physics of the problem. As a simple illustration, in the 1d induction problem, the asymptotic MT mapping yields a 1–1 relationship between the conductance-depth domain and the apparent resistivity-frequency domain. This mapping incorporates the major physics and hence it can be used as an approximate inverse mapping. In face, the use of this mapping in an iterative scheme has been successfully applied by Goldberg, Loewenthal and Rotstein (1982) and it was their paper that helped formulate this particular approach of the general AIM inversion method.

The forward and inverse mapping for the asymptotic equation are

$$\begin{aligned} &\text{FORWARD} \quad \rho_a = \frac{z}{\tau(z)} \qquad \omega = \frac{1}{\mu_0 z \tau(z)} \\ &\text{INVERSE} \quad \tau(z) = \frac{1}{\sqrt{\mu_0 \omega \rho_a(\omega)}} \qquad z = \xi \sqrt{\frac{\rho_a(\omega)}{\mu_0 \omega}}. \end{aligned} \tag{37}$$

ξ is a depth mapping factor which adjusts the inverse mapping. This mapping (without the factor ξ) is often referred to as Bostick/Niblett mapping.

As an illustration of how the mapping can work in a 1d setting, Figure (8) shows the results of applying it to the test model of Whittall and Oldenburg (1990). A value $\xi = 1.2$ was chosen to carry out the inversion. The model constructed at the 6th iteration reproduces all apparent resistivities to within 1% and all phases to within 0.4°.

In applying the AIM approach to the inversion of 2d MT data, Oldenburg and Ellis chose, as an approximate inverse mapping, a composite of 1d inversions carried out at each station. For the example presented here, the following approach is used. At each iteration, the 2d MT responses are computed using the transmission line modelling code supplied by Ted Madden. The same cellularization is used for the inverse problem although the model elements are taken to be log conductivity. $\tilde{\mathcal{F}}^{-1}$ is assigned to be a series of 1d inverse mappings, each of which is formulated as a linear programming problem (Dosso and Oldenburg, 1989). At each station for the nth iteration we desire to invert apparent resistivities and

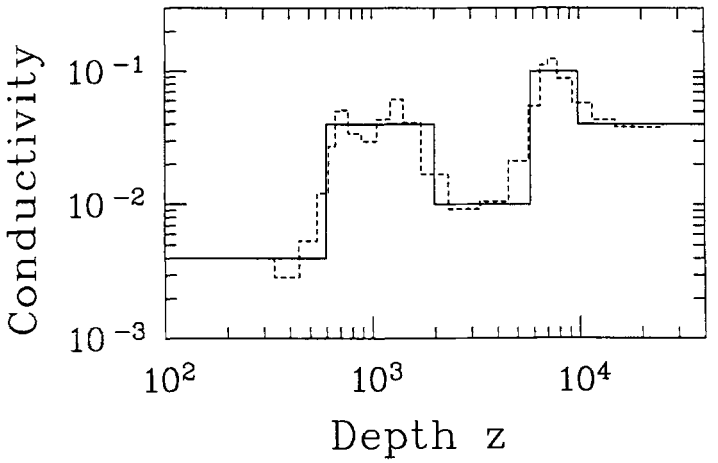

Fig. 8. The AIM inversion is applied to MT data taken from the 1-D structure shown by solid line. Apparent resistivities and phases at 25 frequencies were inverted. The dashed line shows the conductivity structure recovered after 6 iterations.

phases predicted from accurate 2d forward modelling applied to $\sigma^{(n)}(y, z)$. Denote these responses generically as $\mathbf{e}^{(n)}$. Let $\mathbf{c} = (c_1, c_2, \ldots, c_{n_z})$ be the discretized array of log $\sigma(z)$ values in the cells beneath the station of interest. The goal of the 1d inversion is to find a vector $\mathbf{c}$ whose predicted 1d responses are in acceptable agreement with the data $\mathbf{e}^{(n)}$. To carry out this inversion the 1d problem is linearized and written as

$$\sum A_{jk} c_k^{(l)} = e_j^{(n)} - e_j^p + \sum A_{jk} c_k^{(l-1)} + n_j. \tag{38}$$

The index l refers to the iteration number of the 1d inversion. In (38) e_j^p is the datum predicted from a 1d forward modelling applied to $\mathbf{c}^{(l-1)}$, A_{jk} is the integral of the 1d Fréchet derivative over the k'th partition element and n_j is a noise value for the j'th datum. The 1d inverse model is obtained by minimizing

$$\begin{aligned} \phi(\mathbf{c}^{(l)}) = \sum_{j=1}^{N} \left| \frac{n_j}{\varepsilon_j} \right| + W_z \sum_{k=1}^{N_z - 1} w_k |c_{k+1}^{(l)} - c_k^{(l)}| \\ + W_y \sum_{k=1}^{N_z - 1} \eta_k |c_k^{(l)} - \bar{c}_k^{(l-1)}|, \end{aligned} \tag{39}$$

where ε_j is an estimate of the standard deviation of each datum; W_z and W_y are respective weights controlling the tradeoff between misfit, vertical roughness and horizontal roughness, w_k and η_k are partition weightings for the spatial roughness norms, and $\bar{c}_k^{(l-1)}$ is a reference model evaluated from the conductivity structure at nearby stations. The collection of all 1d inversions produces a 2d model estimate $\tilde{m}^{(n)}$ which is subtracted from $\tilde{m}^{\text{obs}}$ to yield the 2d conductivity perturbation. The above procedure can be applied separately or jointly to TE and TM mode data. For

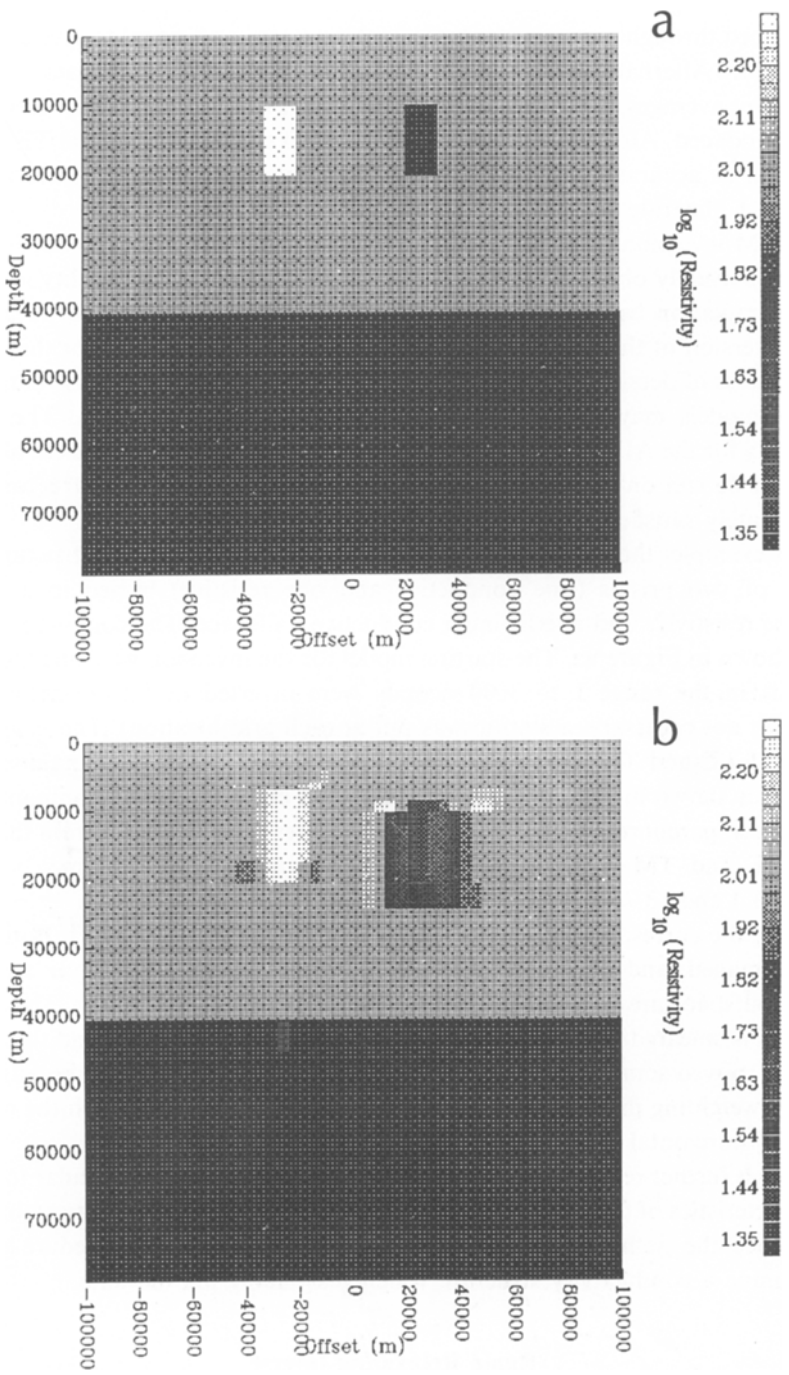

Fig. 9. A conductive prism (10 Ω · m) and resistive prism (1000 Ω · m) buried in a 40 km thick layer of 100 Ω · m, and overlying a 10 Ω · m halfspace is shown in (a). The result of the AIM inversion applied to the Berdichevsky determinant average data is shown in (b).

a joint inversion, at each iteration the perturbation estimates from each data set can be combined through averaging or by extracting a common signal to give a modified perturbation. Alternatively, one can first combine TE and TM mode data to generate determinant averages (Berdichevsky and Demitriev, 1976) and consider these as data to be reproduced. Although this approach is not likely to fit individual TE and TM mode data as accurately as the determinant average data, it may suffice for some examples. I illustrate this in the example shown here.

The AIM inversion is generally very stable and remarkably good reduction in the χ^2 misfit is usually observed during the first few iterations. The stability is inherent in the formulation because a global minimum structure norm is incorporated into the 1d inversion of the approximate inverse mapping. The tradeoff for this stability may be a loss of detailed structure in the constructed model and precise data fits for complex models may not be found. This is not of great concern. The guiding philosophy for the AIM inversion is to produce a computationally efficient algorithm which can be run on a small computer to generate a conductivity structure which approximately satisfies all available data.

As an example, the AIM procedure is applied to a conductivity structure which consists of two prisms (one conductive and one resistive) buried in a layer of moderate resistivity and overlaying a conductive halfspace. The conductivity structure is shown in Figure 9a. The starting model for the inversion was a halfspace and 9 periods in the range 1 to 3000 seconds were inverted at 50 station locations. (Although not necessary, a station was put at each grid location). The determinant average of TE and TM mode data were inverted and the model obtained after 7 iterations is shown in Figure 9b. The r.m.s. misfit error for the determinant data is 2% on the apparent resistivities and 1° on the phases. The responses from this model fit the TE and TM mode apparent resistivities and phases to r.m.s. values of (4.3%, 2.3°) and (3.7%, 1.6°), respectively.

Overall, the correspondence between Figure 9b and a is quite good. Both prisms are well imaged, and the background conductivities in the upper layer and in the bottom halfspace are well approximated. There are artifacts however. The conductive prism is smeared out in both the lateral and vertical directions and the resistive prism has moved somewhat toward the surface. These features result because of the choice of weighting parameters in Equation (39) and the way in which the reference model for horizontal roughness was selected.

Although further research is needed on the AIM approach, in particular to explore the characteristics of the approximate inverse mappings as they relate to stability and convergence, the method is promising. It provides an inexpensive procedure by which to determine a conductivity structure which reasonably fits the data.

Rapid Relaxation Inverse

The more usual approach to solving the inverse problem is to linearize the equations and to map a data misfit directly into a model perturbation. There are

two computationally intensive steps. First, it is necessary to compute the Fréchet derivatives or sensitivities which quantitatively relate changes in the model to changes in the data. This requires a large amount of computation because, irrespective of the method adopted for computing the sensitivities, the forward model equations need to be solved many times. The second computationally intensive operation is the solution of the matrix equation. For the sake of example, suppose that the conductivity model is characterized by 2500 cells; this establishes the number of unknowns. If there are 20 MT stations, each of which has measured impedances (both modes) at 20 frequencies, then the number of (real) data is 1600. The discretized equations

$$G\delta\boldsymbol{\sigma} = \delta\boldsymbol{e}$$

involves a matrix G which is 1600×2500.

The computational complexity of the full linearized solution for even moderate 2d problems has spawned a new approach which appears to have great potential. Smith and Booker (1988) refer to it as Rapid Relaxation Inverse (RRI). Approximate Fréchet derivatives are generated, and 1d inversions are carried out at each site. The effects of lateral changes in conductivity are incorporated by using the 2d electric field to evaluate the approximate Fréchet derivatives. Data for the inversions are the misfit between the observations and the responses obtained from 2d modelling, and the 1d inversions are regularized by minimizing a norm which relates to the curvature energy of the model in both the horizontal and vertical directions.

For brevity, I shall only summarize Smith and Booker's work for the TE mode. They present an analogous formulation for the TM mode. By introducing the variable

$$V = \frac{1}{E}\frac{\partial E}{\partial z} \tag{40}$$

the TE mode differential Equation (4) can be written as

$$\frac{\partial V}{\partial z} + V^2 + \left\{\frac{1}{E}\frac{\partial^2 E}{\partial y^2}\right\} - i\omega\mu_0\sigma = 0. \tag{41}$$

The effect of lateral gradients are determined by the term in brackets. Let $\sigma = \sigma_0$ be a starting model, and let V_0 and E_0 satisfy Equation (41) when $\sigma = \sigma_0$. If the conductivity is perturbed to $\sigma = \sigma_0 + \delta\sigma$, and if the term in brackets in (41) is assumed not to change significantly, then the perturbation for $V(z, \omega)$ becomes

$$\frac{\partial}{\partial z}\delta V + 2V_0\delta V - i\omega\mu_0\delta\sigma = 0. \tag{42}$$

This equation can be solved to yield

$$\partial V(y_j, 0) = \int i\omega\mu_0\left[\frac{E_0(y_j, z)}{E_0(y_j, 0)}\right]^2 \delta\sigma(y_j, z)\, dz \tag{43}$$

where the integration extends from the surface to a depth at which the electric field has decayed to zero. We note that the approximate Fréchet derivative in (43) has the same form as the 1d Fréchet derivative (Oldenburg, 1978; Parker, 1980) and that the change in the surface datum depends only upon the change in the conductivity directly beneath the station. The numerical value of the kernel in (43) differs from that of the 1d solution because the electric fields are those obtained from a precise 2d forward solution. The zeroth-order effects of lateral conductivity change are therefore included, at least for the TE mode.

The inversion proceeds as follows. At each iteration the 2d equations are solved to compute the surface responses and the electric fields at depth. The kernel functions in (43) are evaluated by using these fields. For each station, a norm

$$\int \left[\left\{ \frac{\partial^2}{\partial(\log(z+z_0))^2} + (z+z_0)^{(1/2)}(\Delta y)^{3/2}\alpha \frac{\partial^2}{\partial y^2} \right\} \log(\sigma) \right]^2 \mathrm{d}(\log(z+z_0)) \tag{44}$$

is minimized subject to the data constraints specified in Equation (43). In (44) Δy corresponds to the distance between the two neighbouring stations, α is a variable which controls the relative importance of vertical to horizontal smoothing. The norm is constructed so that the conductivity model and depth coordinate are logarithmic variables. At each iteration the current model is updated with only a percentage of the $\delta\sigma(y, z)$ and the conductivities are interpolated between sites to produce a new $\sigma(y, z)$.

To illustrate the RRI technique I have reproduced an example given by Smith and Booker (1988) and Smith (1988). It is the same conductivity as used in the AIM example (Figure 9). Data for both TE and TM modes for 6 periods between 10 and 320 sec at 23 sites were inverted. The starting model for the inversion was a halfspace. The results of the TE and TM mode inversions after 16 iterations are shown in Figure 10. The rms data misfits are 0.7% for TM and 0.6% for TE. The conductive prism is well imaged for the TE mode, and although the resistive prism is seen, its boundaries are not well located. For the TE mode, the surface responses are related to the anomalous currents. The larger current flowing in the conductor makes this feature more visible than the resistor. In the TM inversion however, the lateral boundaries of both prisms are well imaged. This is in accordance with the charge accumulated on the boundaries.

Overall, the inversion has been fairly successful in delineating the two bodies and background conductivities. As in the AIM inversion in Figure 9b however, the final image shows artifacts. The conductive prism has tails emanating from its boundaries and the TM inversion displays a drop out beneath both prisms.

Linearized Solutions

A traditional approach to solving the inverse problem is based upon linearization of the equations. The iterative analysis begins with an estimated conductivity

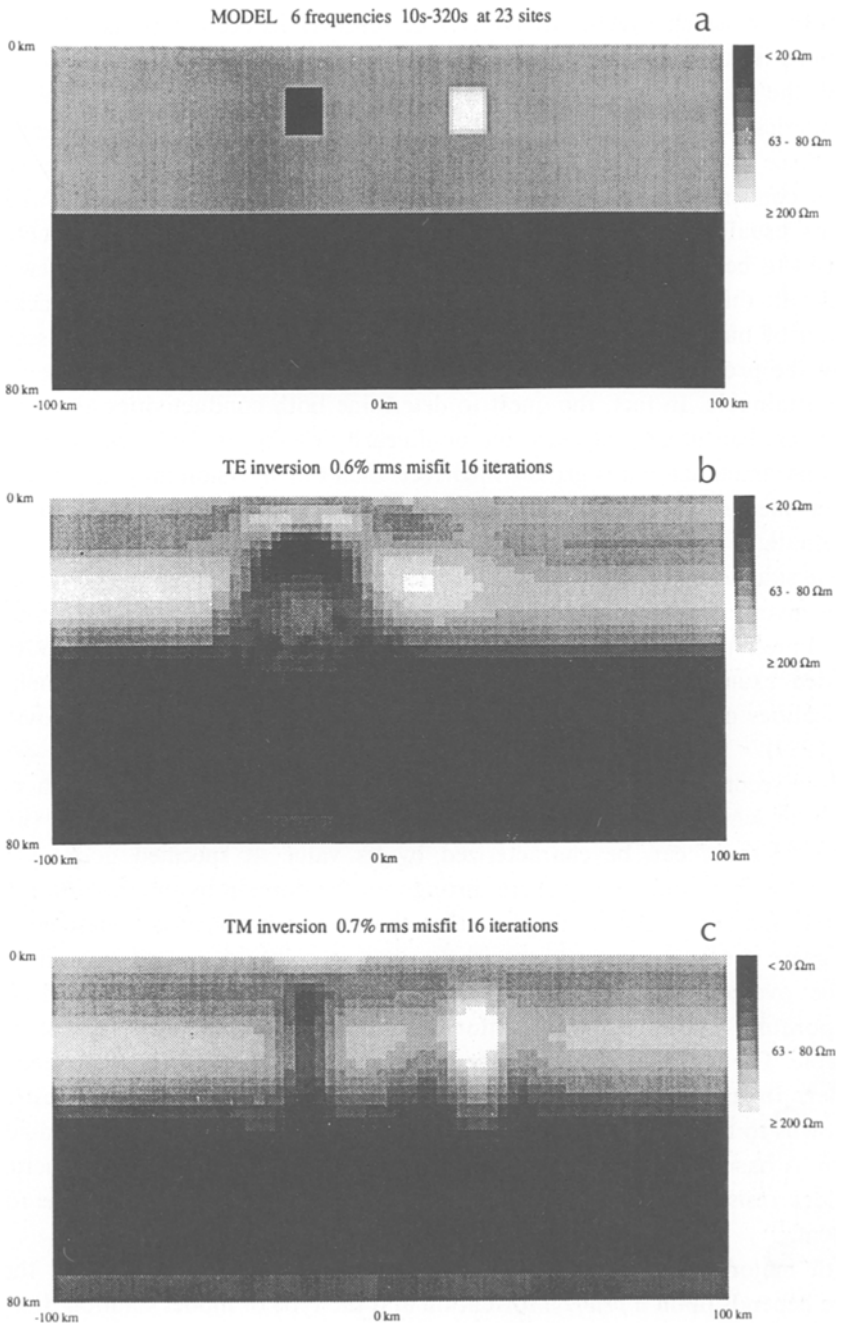

Fig. 10. Rapid Relaxation Inverse of the two prism model. The conductivity model is given in panel (a) and panels (b) and (c) respectively, show the conductivity structures from inverting TE and TM mode data. The figure is extracted from Smith (1988).

structure for which Fréchet derivatives or sensitivities are computed. A system of equations is solved to recover a model perturbation which is added to the starting model; the procedure iterates until some convergence criterion is satisfied.

Numerical computations in the above demand that the model be parameterized. The choice of parameterization is crucial since the nature of the inverse solution and the convergence properties of the algorithm are intimately tied to it. Parameterizations usually fall into one of two categories. In the first, the conductivity is assumed to be geologically simple (for example, a layered earth with a few buried bodies). In this format the conductivities and structural values (layer thicknesses, location of buried bodies) are to be determined. At first sight it might seem that posing the problem in terms of a few parameters would make the inverse solution easily attainable. In fact, the quest to determine both conductivities and structural parameters can greatly increase the nonlinearity of the problem. Moreover, if the model parameterization is grossly incorrect, then the inversion may never be able to recover meaningful information. Much work will have been done to solve a mathematical problem whose answer has little geophysical relevance. On the positive side however, if the earth is parameterized correctly then the nonuniqueness of the inverse problem is greatly restricted and the constructed model may be a good representation of the earth conductivity. Ku (1976) and Rodi (1976) have provided examples of this approach. An in-depth analysis on the benefits and practicalities of using both conductivity and geometric parameters is provided by Pek (1987).

In the second method of parameterization, the earth is divided into a number of cells in which the conductivity of each cell is constant. Equivalently (almost), the conductivity can be characterized by its value at specified nodal locations and can be determined everywhere throughout the domain by interpolation. Generally, the number of cells is large so that the inverse problem is underconstrained. This gives rise to nonuniqueness in the inverse solution, but the nonuniqueness can be overcome by minimizing an appropriate norm of the model and by incorporating additional information about the conductivity structure if it is available. The algorithm generated by Rodi *et al.* (1983) can be implemented in this manner. In an effort to reduce the number of unknowns, and yet restrict the unknowns to be cell conductivities, Jupp and Vozoff (1976) introduced a dual mesh system. A basic mesh (Madden, 1973) is used to delineate the geologic structure and the block resistivities to be determined; a finer mesh is used for solving the forward problem.

Both major types of parameterizations given above have merit, but the final choice depends upon *a priori* information and the type of model solution desired. In some cases a hybrid parameterization is used (Zhdanov and Golubev, 1983; Park, 1987; Mackie *et al.*, 1988). The earth is segmented by major block boundaries (possible moveable) and the interior of each block is represented by many cells or equivalent parameters. Such parameterizations are especially appropriate when modelling regions with known geologic boundaries.

Irrespective of the parameterization, the linearized analysis produces a system of equations

$$G\delta\mathbf{m} = \delta\mathbf{e} \tag{45}$$

where G is the sensitivity matrix, $\delta\mathbf{m}$ is the vector of model perturbations, and $\delta\mathbf{e}$ is a vector of data residuals. For problems of realistic size however, the system of Equations (45) is large and the numerical computations required to generate G and the residual vector $\delta\mathbf{e}$ can be prohibitively expensive and time consuming, even on a large computer. In this review paper, it is therefore worthwhile to present some of the more efficient methods to compute these quantities.

With regard to the calculation of the responses, we can assume that the conductivity model is partitioned into a number of cells and a finite difference or finite element matrix system of equations of the form

$$A\mathbf{f} = \mathbf{s} \tag{46}$$

is solved to obtain the field values $\mathbf{f}$ (either electric or magnetic fields) at the nodal positions. If rectangular prisms are used, and N_y and N_z respectively denote the number of cells in the $\hat{y}, \hat{z}$ directions (for the 2d problem), then the number of unknowns in the problem is $(N_y + 1)(N_z + 1) = N_p$ and the matrix A is $N_p \times N_p$. Fortunately, this matrix is bandlimited and is usually symmetric. This reduces the computational burden and storage requirements for the solution. An efficient solution is effected by decomposing A into the product of an upper and lower triangular matrix $A = LU$ (or LL^T if A is symmetric), and to solve (46) in two steps. First solve $L\mathbf{z} = \mathbf{s}$ for $\mathbf{z}$ by back-substitution, and then solve $U\mathbf{f} = \mathbf{z}$ by forward-substitution to recover $\mathbf{f}$. Although this decomposition standardly involves $4N_yN_z^2$ floating point operations, a rapid technique, based upon the incomplete factorization method (ILU) with orthomin acceleration (Bethie and Vinsome, 1982), offers substantial improvement. Only $40N_yN_z$ computations are required and storage requirements are also reduced (Smith and Booker, 1988).

Regarding computations of the partial derivatives, there are three ways to proceed. The first (and least desirable) is to perturb an individual parameter and then compute the forward responses. The numerical difference between the j'th datum for the perturbed and unperturbed systems yields the estimates for the matric element

$$G_{jk} = \frac{\Delta e_j}{\Delta m_k}. \tag{47}$$

This approach, although conceptually straightforward, suffers from two drawbacks. Computations of the matrix G at each iteration requires $N_yN_zN_f$ forward computations. This can be prohibitive. There is also difficulty in obtaining good estimates for G using a differencing technique (Glenn *et al.*, 1973). The method is not recommended.

The two drawbacks listed above can be overcome by differentiating the initial differential equations with respect to the various parameters and solving for the sensitivities directly (Rodi, 1976; Jupp and Vozoff, 1976; Cerv and Pek, 1981; Hohmann and Raiche, 1988; McGillivray and Oldenburg, 1989). An important advantage of this approach is that the differential equation for the sensitivity is identical (except for the right hand side) to the differential equation for solving the forward problem. If the initial matrix factorization was stored, then the sensitivities can be computed efficiently.

The essential steps in the sensitivity equation method are seen by starting with the forward solution

$$A\mathbf{f} = \mathbf{s}.$$

Differentiate this equation with respect to an unknown parameter m_k. Since the source is independent of the model, $\partial \mathbf{s}/\partial m_k = 0$ and hence

$$A \frac{\partial \mathbf{f}}{\partial m_k} = -\frac{\partial A}{\partial m_k} \mathbf{f}. \tag{48}$$

The right hand side of Equation (48) shows that the field variable at any node is altered by a change in the model. The matrix A is known analytically and $\partial A/\partial m_k$ is easily calculated (there are only a few elements of A which depend upon m_k); $\mathbf{f}$ is known from the forward solution. Equation (48) is easily solved if the LU decomposition of A made in the forward computation is stored.

The remaining step is to compute $\partial e_j/\partial m_k$. The datum e_j generally involves the values of $\mathbf{f}$ at the observation site and also vertical derivatives of the field. For example, in the 2d TE mode, the field vector $\mathbf{f}$ corresponds to the electric field at the nodal points. If the data are the apparent resistivities, then one needs to compute $\partial E/\partial m_k$ and $\partial H/\partial m_k$ and combine them to obtain $\partial \rho_a/\partial m_k$. These computations can be carried out once $\partial \mathbf{f}/\partial m_k$ has been computed. (See Rodi, 1976; Jupp and Vozoff, 1976; or Cerv and Pek, 1981 for details and examples.)

At each iteration, the generation of the matrix Equation (48) involves a forward computation and a factorization of the matrix A. Evaluation of the sensitivity matrix then requires $N_y N_z N_f$ further solutions of the same system of equations but with a different right-hand side. Again, this is efficient if the matrix has been factored.

The second method for computing the sensitivity matrix G in equation (45) makes use of the adjoint equation. This formulation, also referred to as the Green's function approach, has been presented by Weidelt (1975). General formulations for the adjoint equation can be found in Morse and Feshbach (1963), Lanczos (1961), and Roach (1982); detailed derivation for the 3d electromagnetic induction problem has been given by Park (1987). The adjoint solution appears not to be as well known as the sensitivity equation method and for this reason I shall present it in more detail. My formulation follows that of Park (1987) except that it is restricted to the 2d TE mode.

Equation (4) is the basic equation for TE mode induction. Consider two conductivities $\sigma_1(\mathbf{r})$, $\sigma_2(\mathbf{r})$ and two corresponding electric fields $E_1(\mathbf{r})$ and $E_2(\mathbf{r})$ which satisfy

$$\nabla^2 E_1 - i\omega\mu_0\sigma_1 E_1 = 0$$
$$\nabla^2 E_2 - i\omega\mu_0\sigma_2 E_2 = 0. \tag{49}$$

Subtracting these equations yields

$$\nabla^2 \delta E - i\omega\mu_0\sigma_1\delta E = i\omega\mu_0\delta\sigma E_2 \tag{50}$$

where $\delta E = E_2 - E_1$ and $\delta\sigma = \sigma_2 - \sigma_1$. Homogeneous boundary conditions for (50) are applicable on all boundaries ($\partial\delta E/\partial n = 0$ on the top and vertical boundaries and $\delta E = 0$ on the bottom boundary).

To find the adjoint we proceed as follows. First rewrite Equation (50) in a more compact form

$$Du = i\omega\mu_0\delta\sigma E_2$$

where (51)

$$D = (\nabla^2 - i\omega\mu_0\sigma_1)$$

and $u(\mathbf{r})$ is a complex scalar valued function. Let $\mathscr{D}$ denote the adjoint operator and let $v(\mathbf{r})$ be a complex scalar valued function in the domain of $\mathscr{D}$. Then $\mathscr{D}$ is specified by finding the differential operator and associated boundary conditions such that

$$(v, Du) = (u, \mathscr{D}v)^*$$

or (52)

$$\int_A v^* Du \, da = \int_A u\mathscr{D}^* v^* \, da.$$

The complex conjugates are cumbersome, and in addition, a further simplification ensues if we define

$$\tilde{D} = \mathscr{D}^* \quad \text{and} \quad \tilde{v} = v^*. \tag{53}$$

Thus $\tilde{D}$ is the algebraic adjoint of D and $\tilde{v}$ is a scalar valued function in its domain. With these definitions Equation (52) becomes

$$\int \tilde{v} Du \, da = \int u\tilde{D}\tilde{v} \, da. \tag{54}$$

Substitution on the left for Du, and application of Green's second identity, shows that

$$\tilde{D} = \nabla^2 - i\omega\mu_0\sigma_1. \tag{55}$$

It is straightforward to verify that $\tilde{D}$ satisfies the same (homogeneous) boundary conditions as D. This is notable since it means that the adjoint problem can be solved with the same numerical code that was used for the forward problem.

The general adjoint equation is

$$\tilde{D}\tilde{v} = \gamma \tag{56}$$

where $\gamma = \gamma(\mathbf{r})$ is (as yet) an unspecified source function. The differentials for the MT problem are found by appropriately choosing γ in (56) and then using Equation (54). First, substitute δE for u and use Equation (51) to obtain

$$\int_A \delta E(\mathbf{r})\tilde{D}\tilde{v}(\mathbf{r})\, \mathrm{d}a = \int_A \tilde{v}(\mathbf{r})i\omega\mu_0\delta\sigma(\mathbf{r})E_2(\mathbf{r})\, \mathrm{d}a. \tag{57}$$

This is a general equation; we are free to choose whatever source function is useful. From the form of (57) we see that the perturbation at an observation point $\mathbf{r}_0$ could be obtained if the adjoint equations were solved with a delta function source at $\mathbf{r}_0$. That is, $\tilde{v}$ should be the solution of

$$\tilde{D}\tilde{v} = \delta(\mathbf{r} - \mathbf{r}_0). \tag{58}$$

If we denote this solution by $\tilde{v}(\mathbf{r} \mid \mathbf{r}_0)$ then, using the properties of a delta function, we obtain

$$\delta E(\mathbf{r}_0) = i\omega\mu_0 \int_A \tilde{v}(\mathbf{r} \mid \mathbf{r}_0)E_2(\mathbf{r})\delta\sigma(\mathbf{r})\, \mathrm{d}a. \tag{59}$$

This is the desired form except that the electric field E_2 is demanded in the integral. If we make the assumption that δE is small, then $E_2 = E_1 + \delta E$ can be replaced (to first order) by E_1 in the integrand. If the conductivities are constant within each cell, then the sensitivity equation can be written as

$$\delta E(\mathbf{r}_j) = i\omega\mu_0 \sum_k G_{jk}\delta\sigma_k, \tag{60}$$

where

$$G_{jk} = \int_{A_k} \tilde{v}(\mathbf{r} \mid \mathbf{r}_j)E_1(\mathbf{r})\, \mathrm{d}a_k.$$

The sensitivities for the j'th location are therefore computed by solving the adjoint equation once and carrying out the integrals over each cell.

The foregoing shows that the matrix G can be computed by using either the sensitivity equation method or the adjoint method. The choice depends upon the relative number of unknowns compared to the number of data. For the adjoint equation one forward modelling solution and N_s solutions (where N_s is the number of station locations) of the adjoint equation need to be computed for each frequency. Since the adjoint problem uses the same program as the forward modelling, there are $N_f(N_s + 1)$ forward solutions to be computed (N_f is the number of frequencies). This compares with $N_f(N_y N_z + 1)$ forward solutions for the sensitivity equation method. Generally, the adjoint equation method is more computationally efficient but the sensitivity equation method can be economical in those cases where cells are grouped to restrict the number of unknowns.

Having found first order sensitivities, the next step is to compute the model perturbation by solving the equations

$$G\delta\mathbf{m} = \delta\mathbf{e}. \tag{61}$$

At the heart of all computational methods is the realization that the solution to (61) is nonunique and that the matrix equations are ill-conditioned. Minimization of an objective function which includes model characteristics and a misfit to the data can overcome these difficulties. As an example, minimizing

$$\Phi(\delta\mathbf{m}) = \|W_m\delta\mathbf{m}\|^2 + \lambda(\|W_e(\delta\mathbf{e} - G\delta\mathbf{m})\|^2 - \chi^2), \tag{62}$$

where W_m is a weighting matrix for the model elements, W_e is a weighting matrix for the data, and λ is a Lagrange multiplier, will produce a model perturbation that globally misfits the data by a value χ^2 and has a minimum weighted norm. Perturbations having different characteristics can be obtained by altering the weighting matrix W_m and by using different accepted misfit values. There exists a plethora of literature which focuses upon the solution of (62) and convergence of the iterative schemes. It serves little purpose to summarize those works here, even in a review paper. The reader is referred to Jackson, 1972; Jupp and Vozoff, 1974; Weidelt, 1975; Cerv and Pek, 1981; Gill *et al.*, 1981; Menke, 1984; Constable *et al.*, 1987.

The minimization of (62) produces a conductivity perturbation which has a minimum norm structure. However, this normed attribute does not apply to the final conductivity model which fits the data. For instance, successively finding perturbations which have the smallest energy in their first or second derivative does not imply that the final constructed model will share this same attirbute. This is unattractive if the goal is to find a globally minimum structure model. However, a simple reformulation of the perturbation equations, first used to estimate upper and lower bounds to the conductance over arbitrary depth for 1d MT problem (Oldenburg, 1983), can overcome this. The transformation is effected by writing δm in the integral or matrix equations as $\delta m = m_2 - m_1$. Substitution of this into Equation (62) yields

$$G\mathbf{m}_2 = G\mathbf{m}_1 + \delta\mathbf{e}. \tag{63}$$

The left hand side of (63) involves the conductivity model; the right hand side is the modified data. The norm in (62) altered to be

$$\Phi(\mathbf{m}_2) = \|W_m\mathbf{m}_2\|^2 + \lambda(\|W_e(\delta\mathbf{e} + G\mathbf{m}_1 - G\mathbf{m}_2)\|^2 - \chi^2). \tag{64}$$

With appropriate choice of weighting function W_m in Equation (64) it is possible to compute a globally flattest or smoothest model. These models are often desirable since they have minimum structure and hence observed features have a greater likelihood of being representative of structure in the earth. This global norm solution has been used by Constable *et al.* (1987) and by Booker and Smith (1988) with excellent results in 1-D inversions.

A somewhat different formulation for linearized inversion has been proposed by Tarantola and Valette (1982), and Tarantola (1987). The approach, referred to as total inversion, is also called maximum likelihood and stochastic inversion (Franklin, 1970). The technique produces a model which simultaneously minimizes the difference between the observed and predicted data, and the difference between the constructed and an *a priori* conductivity model. In its complete form, this approach can produce substantially different results from that outlined in the previous section. However, when data and model errors are uncorrelated and when Gaussian statistics are assumed, the norm to be minimized is

$$\Phi(\delta \mathbf{m}^{(k)}) = (\delta \mathbf{e} - G_k \delta \mathbf{m}^{(k)})^T R_{dd}^{-1} (\delta \mathbf{e} - G_k \delta \mathbf{m}^{(k)}) + \\ + (\mathbf{m}^{(k)} - \mathbf{m}_0 + \delta \mathbf{m}^{(k)})^T R_{mm}^{-1} (\mathbf{m}^{(k)} - \mathbf{m}_0 + \delta \mathbf{m}^{(k)}) . \quad (65)$$

In Equation (65), R_{dd} is the covariance matrix for the data, R_{mm} is the covariance matrix for the model parameters, $\mathbf{m}_0$ is an *a priori* model, $\mathbf{m}^{(k)}$ is the model at the beginning of the k'th iteration and G_k is the sensitivity matrix. The updated model is obtained by adding $\delta \mathbf{m}^{(k)}$ to $\mathbf{m}^{(k)}$. The two convariance matrices determine the form of the achieved model. In particular, the fluctuations of the final model away from the *a priori* model are controlled by the diagonal terms R_{mm}^{-1} and the roughness is controlled by off-diagonal terms. The relative weighting regarding the tradeoff between fitting the data and producing a model that is close to the *a priori* model is controlled by the norms of the two matrices. Maximum likelihood inversion has been implemented to invert magnetotelluric data over an assumed 2d earth by Mackie *et al.*, (1988), Park (1987), and Neumann and Hermance (1987). The reader is referred to those papers for further details regarding practicalities of setting up the method and convergence of the solution.

Discussion

The last few years have seen significant progress in achieving our goals of solving the electromagnetic inverse problem. The development of more efficient forward modelling schemes like those employing adaptive meshes (e.g., Travis and Chave, 1986) and availability of supercomputers, means that the evaluation of responses from complicated 2d models are now possible. Efficient codes for solving the 3d forward simulation problem are on the horizon. Since the solution of the forward problem plays such a key role in any inversion, this means that numerical linearized inversions will progress quickly. The rapid relaxation inverse of Smith and Booker is already an important step in this regard.

I also expect that new algorithms for solving the inverse problem will arise because of the availability of computer workstations. The output of EMAP processing, the electromagnetic migration and reflectivity imaging techniques, and the AIM inversion are ideally suited to such computational and graphics environments. The inverse problem is nonunique, and in our efforts to invert for

geologically plausible earth structures we will see the next generation of algorithms incorporate more information into the inversion. Not only will this involve satisfying all data from a particular experiment, but information from other experiments (not necessarily electromagnetic) will be included. Interactive, graphics oriented, computing environments are ideally suited to this approach.

In addition to the numerical and new graphics-oriented attacks on the inversion, there has also been substantial progress made in data acquisition. A template for this is EMAP which acquires data along a continuous survey line. Not only does such a survey provide more data, it eliminates interpretation problems that arise from having collected spatially aliased data. As we attempt to solve the 3d problem however, data acquired over an areal survey will be demanded. Such data sets are already in existence in the mining industry where targets are closer to the surface and hence the size of the areal array is limited.

The information attainable from electromagnetic induction studies seems poised to take a major step forward. With large field data sets of improved quality, with improved methods in data processing, and with improved and new methods for imaging/inverting the data, it is anticipated that major advances in electromagnetic interpretation and results will be evident by the time of the next electromagnetics workshop.

Acknowledgements

This review would not have been possible without the kind assistance of many individuals. Special thanks is extended to Ted Madden, Steve Park, Carlos Torres-Verdin, Phil Wannamaker, Peter Weidelt, Torquil Smith, John Booker, V. Cerv and J. Pek who supplied basic material used in this review. My daily interaction with Rob Ellis and his input into many of the areas covered in this review are gratefully acknowledged.

References

Behie, A. and Vinsome, P. K. W.: 1982, 'Block Iterative Methods for Fully Implicit Reservoir Simulation', *Soc. Pet. Eng. J.* 658–668.

Berdichevsky, M. N. and Dmitriev, V. I.: 1976, 'Basic Principle of Interpretation of Magnetotelluric Sounding Curves. in A. Adam (ed.), *Geoelectric and Geothermal Studies*, KAPG Geophysics Monogr., Akademiai Kiado, Budapest, pp. 165–211.

Berdichevsky, M. N. and Zhdanov, M. S.: 1984, *Advanced Theory of Deep Geomagnetic Sounding*, Elsevier, 408 pp.

Bostick, F. X. Jr.: *Electromagnetic Array Profiling (Expanded Abstract)*, Soc. Expl. Geophys. 56th Ann. Mtg. Houston, TX.

Cerv, V. and Pek, J.: 1981, 'Numerical Solution of the Two-Dimensional Inverse Geomagnetic Induction Problem', *Studia geoph. et geod.* **25**, 69–80.

Chave, A. D and Brooker, J. R.: 1987, 'Electromagnetic Induction Studies', *Rev. Geophys.* **25**, 989–1003.

Claerbout, J. F.: 1976, *Fundamentals of Geophysical Data Processing*, McGraw-Hill Book Co.

Constable, S. C., Parker, R. L., and Constable, C. G.: 1987, 'Occam's Inversion: A Practical Algorithm for Generating Smooth Models from Electromagnetic Sounding Data', *Geophys.* **52**, 289–300.

Dosso, E. E. and Oldenburg, D. W.: 1989, 'Linear and Nonlinear Appraisal Using Extremal Models of Bounded Variation', *Geophys. J. Int.* **99**, 483–495.

Flores, C., Kurtz, R. D., and DeLaurier, J.: 1985, 'Magnetotelluric Exploration in the Meager Mountain Geothermal Area', *Canada, Acta Geodaet Geophys. et. Montanist Hung.* **20**, 165–171.

Franklin J. N.: 1970, 'Well-Posed Stochastic Extensions of Ill-Posed Linear Problems', *J. Math. Anal. Appl.* **31**, 682–716.

Gill, P. E., Murray, W., and Wright, M. H.: 1981, *Practical Optimization*, Academic Press.

Glenn, W. E., Ryu, J., Ward. S. H., Peeples, W. J., and Phillips, R. J.: 1973, 'The Inversion of Vertical Magnetic Dipole Sounding Data', *Geophys.* **38**, 1109–1129.

Goldenberg, S., Loewenthal, D., and Rotstein, Y.: 1982, 'An Improved Algorithm for Magnetotelluric and Direct Current Data Interpretation', *J. Geophys.* **50**, 151–158.

Gomez-Trevino, E.: 1987, 'Nonlinear Integral Equations for Electromagnetic Inverse Problems', *Geophys.* **52**, 1297–1302.

Goupillaud, P. L.: 1961, 'An Approach to Inverse Filtering of Near Surface Layer Effects from Seismic Records', *Geophysics* **26**, 754–760.

Hermance, J. F.: 1983, 'Electromagnetic Induction Studies', *Rev. Geophysics* **21**, 652–664.

Hohmann, G. W. and Raiche, A. P.: 1988, 'Inversion of Controlled Source Electromagnetic Data', in M. N. Nabighian (ed.), *Electromagnetic Methods in Applied Geophysics*, Vol. 1, Theory, Soc. Expl. Geophys.

Jackson, D. D.: 1972, 'Interpretation of Inaccurate, Insufficient, and Inconsistent Data', *Geophys. J. R. Astr. Soc.* **28**, 97–109.

Jones, A. G., Kurtz, R. D., Oldenburg, D. W., Boerner, D. E. and Ellis, R. G.: 1988, 'Magnetotelluric Observations along the LITHOPROBE Southeastern Canadian Cordilleran Transect', *Geophys. Res. Let.* **15**, 677–680.

Jupp, D. L. B. and Vozoff, K.: 1974, 'Stable Iterative Methods for Inversion of Geophysical Data', *Geophys. J. R. Astr. Soc.* **42**, 957–976.

Jupp, D. L. B. and Vozoff, K.: 1976, 'Two-Dimensional Magnetotelluric Inversion', *Geophys. J. R. Astr. Soc.* **50**, 333–352.

Ku, C. C.: 1976, 'Inverse Magnetotelluric Problems, *Geophysics* **41**, 276–286.

Kunetz, G.: 1972, 'Processing and Interpretation of Magnetotelluric Soundings', *Geophysics* **37**, 1005–1021.

Kurtz, R. D., DeLaurier, J. M., and Gupta, J. C.: 1986, 'A Magnetotelluric Sounding Across Vancouver Island Detects the Subducting Juan de Fuca Plate', *Nature* **321**, 596.

Lanczos, C.: 1961, *Linear Differential Operators*, Van Nostrand Company Ltd.

Lee, S., McMechan, G. A., and Aiken, G. L. V.: 1987, 'Phase Field Imaging of Electromagnetic Data', *Geophysics* **52**, 678–693.

Levy, S., Oldenburg, D., and Wang, J.: 1988, 'Subsurface Imaging Using Magnetotelluric Data', *Geophysics* **53**, 104–117.

Madden, T. R.: 1973, *Instruction Manual for EDCDC and EMUVA (EMCAL)*, Exploration Aids Inc., Needham, Mass.

Mackie, R. L., Bennett, B. R., and Madden, T. R.: 1988, 'Long Period Magnetotelluric Measurements near the Central California Coast: A Land Locked View of the Conductivity Structure Under the Pacific Ocean', (submitted to *Geophysical Journal*).

McGillivray, P. R. and Oldenburg, D. W.: 1990, 'Methods for Calculating Fréchet Derivatives and Sensitivities for the Nonlinear Inverse Problem – A Comparative Study', accepted in *Geophys. Prospecting*.

Marquardt, D. W.: 1963, 'An Algorithm for Least Squares Estimation of Non-Linear Parameters', *J. SIAM* **11**, 431–441.

Menke, W.: 1984, *Geophysical Data Analysis: Discrete Inverse Theory*, Academic Press.

Morse, P. W. and Feshbach, H.: 1953, *Methods of Theoretical Physics*, McGraw-Hill.

Neumann, G. A. and Hermance, J. F.: 1987, *A Comparison of Four Generalized Inverse Algorithms Using Synthetic Data*, Paper at IUGG meeting, Vancouver, Canada.

Oldenburg, D. W.: 1978, 'One-Dimensional Inversion of Natural Source Magnetotelluric Observations', *Geophysics* **44**, 1218–1244.

Oldenburg, D. W.: 1983, 'Funnel Functions in Linear and Nonlinear Appraisal', *J. Geop. Res.* **88**, 7387–7398.

Oldenburg, D. W. and Ellis, R. G.: 1990, 'Inversion of Geophysical Data Using an Approximate Inverse Mapping', submitted to *Geophysical J. Int.*

Park, S. K.: 1987, *Inversion of Magnetotelluric Data for Multi-Dimensional Structures*, IGPP Report, 87/6, University of California, Riverside.

Parker, R. L.: 1980, 'The Inverse Problem of Electromagnetic Induction: Existence and Construction of Solutions Based upon Incomplete Data', *J. Geophys. Res.* **85**, 4421–4428.

Pek, J.: 1987, 'Numerical Inversion of 2-D MT Data by Models with Variable Geometry', *Phys. Earth and Planet Inter.* **45**, 193–203.

Ranganayaki, R. P.: 1984, 'An Interpretive Analysis of Magnetotelluric Data', *Geophysics* **49**, 1730–1748.

Roach, G. F.: 1982, *Green's Functions*, Cambridge University Press.

Rodi, W. L.: 1976, 'A Technique for Improving the Accuracy of Finite Element Solutions for MT Data', *Geophys. J. R. Astr. Soc.* **44**, 483–506.

Rodi, W. L., Swanger, H. J., and Minster, J. B.: 1983, *ESP/MT: An Interactive System for Two-Dimensional Magnetotelluric Interpretation*, SEG Extended Abstract, p. 151.

Smith, J. T. and Booker, J. R.: 1988, 'Magnetotelluric Inversion for Minimum Structure', *Geophysics* **53**, 1565–1576.

Smith, J. T. and Booker, J. R.: 1988b, *Two and Three Dimensional Inversion of Magnetotelluric Data*, (presented at Ensenada workshop, June, 1988).

Smith, J. T.: 1988, 'Rapid Inversion of Multi-Dimensional Magnetotelluric Data', Ph.D. thesis, Geophysics Program, University of Washington.

Stratton, J. A.: 1941, *Electromagnetic Theory*, McGraw-Hill, 615 pp.

Szaraniec, E.: 1976, 'Fundamental Functions for Horizontally Stratified Earth', *Geop. Prosp.* **24**, 528–548.

Tarantola, A.: 1987, *Inverse Problem Theory*, Elsevier, 613 pp.

Tarantola, A. and Valette. B.: 1982, 'Generalized Nonlinear Problems Solved Using the Least-Squares Criterion', *Rev. Geophys. Space Phys.* **20**, 219–232.

Torres-Verdin, C.: 1985, 'Implications of the Born Approximation for the Magnetotelluric Problem in Three-Dimensional Environments', MSc. Thesis, University of Texas at Austin, TX.

Torres-Verdin, C. and Bostick, F. X. Jr.: 1988, 'Principles of Spatial Surface Electric Field Filtering in Magnetotellurics: The EMAP Technique, (submitted to *Geophysics*).

Travis, B. J. and Chave, A. D.: 1986, *A Moving Finite Element Model for 2-D Magnetotelluric Analysis*, 8th workshop on Electromagnetic induction in the earth and moon, University of Neuchatel.

Varentsov, IV. M.: 1983, 'Modern Trends in the Solution of Forward and Inverse 3-D Electromagnetic Induction Problems', *Geophys. Surv.* **6**, 55–78.

Velikhov, Y. P., Zhdanov, M. S., and Frenkel, M. A.: 1987, 'Interpretation of MHD-Sounding Data from the Kola Peninsula by the Electromagnetic Migration Method', *Phys. Earth Planet Int.* **45**, 149–160.

Vozoff, K.: 1986, *Magnetotelluric Methods*, Geophysical Reprint series No. 5, Soc. Expl. Geophys.

Wannamaker, P. E., Hohmann, G. W., and Ward, S. H.: 1984, 'Magnetotelluric Responses of Three-Dimensional Bodies in Layered Earths', *Geophysics* **49**, 1517–1533.

Wannamaker, P. E., Stodt, J. A., and Rijo, L.: 1985, *PW2D-Finite Element Program for Two-Dimensional Earth Resistivity Structure: User Documentation*, University of Utah, Res. Inst. Rep. ESL-158.

Ward, S. H. and Hohmann, G. W.: 1988, 'Electromagnetic Theory for Geophysical Applications', in Nabighian, M. N. (ed.), *Electromagnetic Methods in Applied Geophysics*, Soc. Expl. Geophys.

Weidelt, P.: 1975, 'Inversion of Two-Dimensional Conductivity Structures', *Phys. Earth and Planet Int.* **10**, 282–291.

Whittall, K. P. and Oldenburg, D. W.: 1990, 'Inversion of Magnetotelluric Data over a One-Dimensional Earth', (to be published in an SEG monograph on magnetotellurics edited by P. Wannamaker).

Zhdanov, M. S.: 1987, 'Application of Space Analysis of Electromagnetic Fields to Investigation of the Geoelectrical Structure of the Earth', *Pageoph* **125**, 483–497.

Zhdanov, M. S. and Golubev, N. G.: 1983, 'Use of Finite Functions Method for the Solution of the 2-D Inverse Problem', *J. Geomag, Geoelectr.* **35**, 707–722.

Zhdanov, M. S. and Frenkel, M. A.: 1982, *The Solution of the Inverse Problems on the Basis of Analytical Continuation of the Transient Electromagnetic Field in Reverse Time*, presented at the 6th Workshop on EM-induction in the earth and moon, University of Victoria.

Zhdanov, M. S. and Frenkel, M. A.: 1983, 'The Solution of the Inverse Problems on the Basis of Analytical Continuation of the Transient Electromagnetic Field in Reverse Time', *J. Geomag, Geoelectr.* **35**, 747–765.